IEEE Access
Multidisciplinary | Rapid Review | Open Access Journal

Received January 23, 2021, accepted February 27, 2021, date of publication March 2, 2021, date of current version March 24, 2021.

Digital Object Identifier 10.1109/ACCESS.2021.3063410

Robust Wideband DOA Estimation Based on Element-Space Data Reconstruction in a Multi-Source Environment

CHUANQI ZHU, (Student Member, IEEE), SHILIANG FANG, QISONG WU, LIANG AN, AND XINWEI LUO

Key Laboratory of Underwater Acoustic Signal Processing, Ministry of Education, Southeast University, Nanjing 210096, China

Corresponding authors: Chuanqi Zhu (chuanqizhu@seu.edu.cn) and Shiliang Fang (slfang@seu.edu.cn)

This work was supported in part by the National Natural Science Funds of China under Grant 11874109, Grant 11574048, Grant 11674057, Grant 11604048, Grant 11704069, Grant 61701109, and Grant 91938203; in part by the Fundamental Research Funds for the Central Universities under Grant 2242020K30044; in part by the Science and Technology on Sonar Laboratory under Grant 6142109180202; and in part by the National Defense Basis Scientific Research Program of China under Grant JCKY2019110C143.

ABSTRACT In the presence of multiple sources, the performance of direction-of-arrival (DOA) estimation based on beam power maximization is susceptible to the energy leaking from the interference beams to the target beam, especially in the case that the signal of interest (SOI) is quite weak. To address this issue, a robust wideband DOA estimation method is proposed in this paper. Unlike those conventional high-resolution methods which mitigate the influence of energy leakage by reducing beamwidths and sidelobe levels, the proposed method achieves this by directly reconstructing the element-space data to approach the received hydrophone data of the single-source scenario containing only the SOI. Element-space data reconstruction (ESDR) for the SOI is achieved by removing the element-space waveforms of all the interference signals from the received hydrophone data. Moreover, an iterative algorithm is developed to adaptively extract the element-space waveform of each interference signal, without requiring the prior information of the array amplitude response coefficients and hydrophone coordinates of a distorted towed array. Simulation results show that the proposed method outperforms its counterparts in terms of estimation accuracy for a multi-source scenario. Meanwhile, the DOA estimation performance of the proposed method in a multi-source environment is close to that obtained by the beam power maximization method in the single-source scenario, even if the signal-to-interference ratio (SIR) is as low as -25 dB. At-sea experimental results prove that, even though the number of signal sources is as many as seven and the SOI is contaminated by real ocean ambient noise, the proposed method still achieves a better DOA estimation performance compared to existing state-of-the-art methods.

INDEX TERMS Distorted towed array, element-space waveform estimation, energy leakage, multi-source environment, wideband direction-of-arrival (DOA) estimation.

I. INTRODUCTION

Direction-of-arrival (DOA) estimation for the weak signals in a multi-source environment is a crucial problem in array signal processing [1]–[3], and plays a significant role in many applications such as sonar, radar, and wireless communication [4]–[6]. Conventional beamforming CBF) is a popular technique for sonar signal processing due to its robustness and effectiveness, and is commonly used in DOA estimation based on beam power maximization [7]. However, in the presence of multiple sources, the performance of DOA estimation is severely affected by the energy leaking from the interference beams to the target beam, due to the wide beams and high-level sidelobes of CBF. The leaked energy can pollute the beam power peak in the target directions or even mask the weak targets directly, and thus degrade the DOA estimation performance.

During the last several decades, many high-resolution DOA estimation methods have been proposed to mitigate the influence of energy leakage by decreasing the beamwidths and sidelobe levels. The minimum-variance distortionless response (MVDR) based approaches and multiple signal

The associate editor coordinating the review of this manuscript and approving it for publication was Jiajia Jiang.

classification (MUSIC) based methods are regarded as the representative methods in the field [8], [9]. These methods obtain narrow beams and low sidelobes but require moderately high signal-to-noise ratio (SNR) and sufficient snapshots to achieve satisfactory performance. For the MUSIC based techniques, the number of sources is also required to be known a priori to separate the signal vectors from the noise vectors. Recently, the technique of sparse reconstruction (SR) provides a new perspective for DOA estimation, due to the spatial sparsity that signal sources of interest only occupy a small part of the entire angular space [10]–[22]. This type of algorithm recovers the spatial distribution of the signal sources by directly representing the array output on an overcomplete basis under sparsity constraint, and is less sensitive to SNR and the number of snapshots [10]–[12]. Several algorithms, such as l_1-norm based singular value decomposition (l_1-SVD) [13] and basis pursuit denoising (BPDN) [14], have directly addressed the sparsity-based DOA estimation problem. However, both the l_1-SVD and the BPDN methods have to choose an appropriate regularization parameter to balance the noise level and sparsity of the signal sources, which is a difficult problem in practice. Several improved sparsity-inducing methods have been proposed to achieve better estimation performance by exploiting the group sparsity that signals at different targets from different directions share the same spectrum [15], [16]. The off-grid version of the sparse Bayesian learning based relevance vector machine (SBLRVM) algorithm [17] and the off-grid sparse Bayesian learning algorithm based on Taylor series expansion (OGSBL-T) [18] have been proposed to achieve accurate DOA estimation in scenarios where the actual signal DOAs are not exactly aligned with the angular grids. The Bayesian sparse-plus-low-rank (BSPLR) matrix decomposition method has been proposed to estimate both stationary and time-varying DOAs by considering all snapshots together rather than estimating the DOAs snapshot-by-snapshot [19], [20]. The method named wideband covariance matrix sparse representation (W-CMSR) has been proposed to estimate the DOAs of wideband signals by representing the array output covariance matrix under sparsity constraints [21], [22]. Although these SR based methods can acquire improved DOA estimation performance, the prior knowledge of the array shape is often requisite.

A passive sonar array often requires a large aperture, even up to several kilometers, to achieve accurate localization and high array gain [23]. This long aperture is typically formed by trailing a hydrophone array behind a towing platform in a nominally straight line [24]. In this case, the forces caused by oceanic currents and internal waves can change the shape of the towed array to some extent [25]. Thus, array shape distortion is inevitable for the towed array. Moreover, the towing platform noise is a strong interference that has to be dealt with for the towed array sonar, due to the limited distance between the towing platform and the towed array [26]. However, most of the aforementioned high-resolution DOA estimation algorithms are known to be sensitive to the model mismatch, such as array shape distortion. Such model mismatch would drastically deteriorate the DOA estimation performance [7]. A number of robust algorithms have been proposed to alleviate this problem [7], [27], [28]. For example, the robust Capon beamformer (RCB) algorithm has been developed by coupling the covariance fitting formulation with an ellipsoidal array steering vector (ASV) uncertainty set [27]. It belongs to the category of diagonal loading methods and the amount of diagonal loading can be exactly calculated based on the ellipsoidal uncertainty set. The wideband RCB (WBRCB) algorithm has been developed by extending the narrowband RCB to the wideband scenario and reducing the computational complexity with a steered covariance matrix technique [28]. The dCv method concerns the CBF beam power as the convolution of the beam pattern with the sources (bearing) distribution, and deconvolves the CBF beam power using a Richardson-Lucy (R-L) algorithm to obtain the bearing distribution of signal sources [7]. These algorithms try to acquire narrow beams and low sidelobe levels while maintaining robust to the model mismatch, which decrease the energy leaking from the interference beams to the target beam. However, the influence of energy leakage still exists as long as the sidelobes are not reduced to a negligible level, and increases with the increasing strength of interference signals. When the signal of interest (SOI) is quite weak, the strong interferences, such as towing platform noise, would drastically decay the DOA estimation accuracy or even mask the weak signals directly [29], [30].

Several algorithms have been proposed to remove the interference signals directly. For example, the CLEAN algorithm has been developed to reduce the sidelobe effect by eliminating the interference signals one by one, in order of descending strength [31]–[33]. The inverse space filtering (ISF) technique has been developed to suppress the interference signal at the hydrophone level [34]. It contains three steps: 1) obtain the tracking beam data of the interference signal utilizing CBF, 2) estimate the element-space waveform of the interference signal based on the nominal array configuration and estimated DOA, and 3) subtract the element-space waveform from the received hydrophone data. The method proposed in [35] combines the technique of CLEAN and ISF to achieve weak target detection in passive sonar. It sequentially removes the interference signals from the received hydrophone data in order of descending strength, one at a time, until the SOI is detected from the updated element-space data. However, assumptions of the distortionless array shape and consistent array amplitude response frequently mismatch those of the actual towed array. Besides, during the sequential signal removal, the estimation accuracy of element-space waveforms of the previously detected interference signals are also affected by the signals that have not yet been detected. Thus, the element-space waveforms of interference signals are not properly removed, which can degrade the DOA estimation accuracy of the SOI to some extent. Hence, DOA estimation for the weak signals in a multi-source environment is still an open problem, particularly when the

array shape distortion and array amplitude response inconsistency coexist.

In this paper, a robust wideband DOA estimation method is proposed to obtain the accurate bearings of the weak signals in a multi-source environment. Unlike those conventional high-resolution algorithms that alleviate the energy leakage by reducing beamwidths and sidelobe levels, the proposed method achieves this by directly reconstructing the element-space data to approach the received hydrophone data of the single-source scenario containing only the SOI. The proposed method contains two distinct stages. In the first stage, the strongest signal is firstly detected based on the CBF method, and its corresponding element-space waveform is estimated and extracted; then the element-space waveforms of other signals are sequentially estimated by removing the previously extracted element-space waveform, until no signal can be detected from the updated sample sequence of beam power. In the second stage, element-space data reconstruction (ESDR) for the signal currently concerned is firstly performed by removing the element-space waveforms of all other detected signals from the received hydrophone data; next, a refined estimate of DOA for the signal currently concerned can be obtained based on the reconstructed element-space data; then, the element-space waveform of the current signal is updated based on the reconstructed element-space data and the refined estimate of DOA, and used for ESDR of the subsequential weaker signals. In addition, a data-driven algorithm is developed for both stages to adaptively acquire the element-space waveform of each detected signal, without requiring the prior information of the array amplitude response coefficients and hydrophone coordinates of a distorted towed array.

The performance of the proposed method is verified by both simulation and at-sea experiments. In conclusion, it offers the following advantages over existing state-of-the-art methods.

1) It outperforms existing algorithms in terms of estimation accuracy. The DOA estimation performance of the proposed method in a multi-source environment is close to that obtained by the beam power maximization method in the single-source scenario.
2) It can still obtain an excellent DOA estimation performance, even if the signal-to-interference ratio (SIR) is as low as -25 dB. In contrast, the DOA estimation performance of the high-resolution algorithms, such as WBRCB and dCv, is severely degraded in this case.
3) It is robust to array shape distortion and array amplitude response inconsistency.

The remainder of this paper is organized as follows. First, Section II introduces the data model and problem background. Next, the proposed ESDR-based wideband DOA estimation method is presented in Section III. Then, experiments based on the simulated and real data are provided in Sections IV and V, respectively, to demonstrate the superiority of the proposed method. Finally, Section VI concludes the paper.

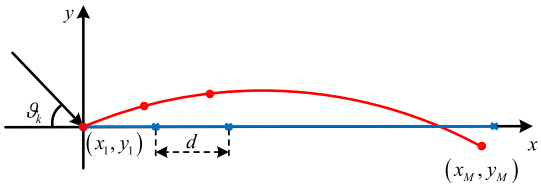

FIGURE 1. Shape distortion of a towed array.

Notations: We use lower-case bold characters to represent vectors, $(\cdot)^T$ denotes transpose, $(\cdot)^H$ denotes conjugate transpose, int $(\cdot)$ expresses rounding to an integer and $x^{(q)}$ stands for the value of x in iteration step q, respectively.

II. DATA MODEL AND PROBLEM BACKGROUND

This section begins with a brief introduction of the data model in a distorted towed array with inconsistent amplitude response. Then, an analysis of wideband DOA estimation based on beam power maximization is presented, followed by a discussion of performance degradation caused by energy leakage in a multi-source environment.

A. DATA MODEL FOR A DISTORTED TOWED ARRAY WITH INCONSISTENT AMPLITUDE RESPONSE

Consider a uniform linear array (ULA) comprising of M elements with inter-element spacing d. Because of oceanic currents and internal waves, the hydrophone array towed behind a maneuvering platform cannot be kept as a straight line, as shown in Fig. 1. Suppose that the array shape distortion only occurs on the horizontal plane. Take the position of the hydrophone nearest from the platform as the origin of the coordinate system. The positive x-axis is defined as the direction opposite the heading of the towing platform.

Sinusoidal array shape distortion is the most common distortion form and can be described as

$$y = A \sin(gx), \tag{1}$$

where A and g are a pair of parameters for describing shape distortion [36]. The x-coordinate of each element of the towed array can be recursively obtained as

$$x_m = \begin{cases} 0, & m = 1, \\ x_{m-1} + \Delta x_m, & m = 2, \ldots, M, \end{cases} \tag{2}$$

where $\Delta x_m = d \Big/ \sqrt{1 + A^2 g^2 \cos^2(g x_{m-1})}$ is the x-coordinate offset between the $(m-1)$th and mth elements [36]. The corresponding y-coordinate can then be obtained according to (1). The element coordinates (x_m, y_m) of the distorted array are denoted by red circles "•" in Fig. 1 as opposed to that of the original linear array ($A = 0$) denoted by blue crosses " ×".

Suppose that K uncorrelated wideband signals originated from far-field sources simultaneously impinge on the towed

array with directions $\boldsymbol{\vartheta} = [\vartheta_1, \ldots, \vartheta_K]$. The data received by the mth element can be expressed as [37]

$$r_m(t) = \alpha_m \left[\sum_{k=1}^{K} s_k\left(t - \tau_{m,k}\right) + v_m(t) \right], \tag{3}$$

where α_m represents the amplitude response coefficient of the mth element, $s_k(t)$ denotes the waveform of the kth signal at a reference position, $\tau_{m,k}$ stands for the time-delay of the kth signal when propagating from the reference position to the mth element, and $v_m(t)$ is the additive noise uncorrelated with the signals, respectively. The term $r_m(t)$ represents the element-space data at the mth hydrophone, to help distinguish it from the beam-space data, while $h_{m,k}(t) = \alpha_m s_k\left(t - \tau_{m,k}\right)$ denotes the element-space waveform of the kth signal component at the mth hydrophone. As shown in Fig. 1, the incident angle ϑ_k is defined as the angle between the incident direction and the negative x-axis. When the first element is considered as the reference, $\tau_{m,k}$ is given by

$$\tau_{m,k} = \frac{x_m \cos\vartheta_k - y_m \sin\vartheta_k}{c}, \tag{4}$$

where c represents the acoustic speed in water. Due to imperfect manufacturing in practice, amplitude response inconsistency is really common for a hydrophone array [38]. Suppose that the amplitude response coefficient of the mth element satisfies a Gaussian distribution

$$\alpha_m \sim \mathcal{N}\left(\mu_\alpha, \sigma_\alpha^2\right), \tag{5}$$

where $\mu_\alpha = \frac{1}{M}\sum_{m=1}^{M}\alpha_m$ represents the mean of the amplitude response coefficients of the hydrophone array and $\sigma_\alpha^2 = \frac{1}{M}\sum_{m=1}^{M}(\alpha_m - \mu_\alpha)^2$ denotes the corresponding variance.

Assuming that N snapshots are collected, the received data $r_m(t)$ can be decomposed into N narrowband components using Discrete Fourier Transform (DFT). The resulting narrowband component corresponding to the nth frequency bin is given by

$$R_m(f_n) = \alpha_m \left[\sum_{k=1}^{K} S_k(f_n)\, e^{-j2\pi f_n \tau_{m,k}} + V_m(f_n) \right], \tag{6}$$

where $n \in [1, \ldots, N]$ represents the discrete frequency index, $f_n = (n-1)f_s/N$ denotes the central frequency of the nth bin with a sampling rate f_s, and $R_m(f_n)$, $S_k(f_n)$, and $V_m(f_n)$ are the DFT coefficients of the received data, wideband signal, and additive noise at the nth frequency bin, respectively. One of the primary goals of most array processing techniques is to estimate the target directions based on (6). Assuming that $K = 2$ and the first source is the target, the second one is the interference. Besides, the noises received by different hydrophones have the same power spectrum, i.e., $V_m(f_n) = V(f_n)$ $(\forall m)$. The Cramer-Rao lower bound (CRLB) for DOA estimation of the wideband signal with a ULA satisfies [39], [40]

$$\begin{aligned} &\mathrm{var}\left(\hat{\vartheta}_1\right) \\ &\geq \frac{1}{(2\pi)^2 T\left(d/c\right)^2 \sin^2\vartheta_1} \\ &\quad \times \frac{1}{\int_{f_l}^{f_h} f^2 \left[\frac{\lambda_1 \frac{S_1^2(f)}{V^2(f)} \frac{S_2^2(f)}{V^2(f)}}{D^2(f,\vartheta_1,\vartheta_2)} + \frac{\lambda_2 \frac{S_1^2(f)}{V^2(f)}}{D(f,\vartheta_1,\vartheta_2)} + \frac{\lambda_3 \frac{S_1^2(f)}{V^2(f)} \frac{S_2(f)}{V(f)}}{D(f,\vartheta_1,\vartheta_2)} \right] df}, \end{aligned} \tag{7}$$

where f_l and f_h respectively represent the lower and upper bounds of the analysis frequency band, $T = N/f_s$ denotes the time analysis window length, $\lambda_1, \lambda_2, \lambda_3$, and $D(f, \vartheta_1, \vartheta_2)$ are respectively given by

$$\begin{aligned} \lambda_1 &= 4\left\{ \sum_{m=1}^{M-1} (M-m)\, m \sin(m\varphi) \right\}^2, \\ \lambda_2 &= 2\sum_{m=1}^{M-1} (M-m)\, m^2, \\ \lambda_3 &= 2(M-2)\sum_{m=1}^{M-1} (M-m)\, m^2 \left[1 + \cos(m\varphi)\right] \\ &\quad -4\sum_{m=2}^{M-1}\sum_{g=1}^{m-1} (M-m)\left[m^2 \cos(g\varphi) + g^2 \cos(m\varphi) \right. \\ &\quad \left. + (m-g)^2 \cos(g\varphi) \right], \\ D(f, \vartheta_1, \vartheta_2) &= 1 + M\frac{S_1(f)}{V(f)} + M\frac{S_2(f)}{V(f)} + M(M-1)\frac{S_1(f)}{V(f)}\frac{S_2(f)}{V(f)} \\ &\quad -2\frac{S_1(f)}{V(f)}\frac{S_2(f)}{V(f)}\sum_{m=1}^{M-1} (M-m)\cos(m\varphi), \end{aligned}$$

and $\varphi = 2\pi f d\left(\cos\vartheta_1 - \cos\vartheta_2\right)/c$.

B. BEAM POWER MAXIMIZATION BASED DOA ESTIMATION AND PERFORMANCE DEGRADATION CAUSED BY ENERGY LEAKAGE IN A MULTI-SOURCE ENVIRONMENT

CBF is a popular technique for array signal processing due to its robustness and effectiveness. Thus, it is commonly used in DOA estimation based on beam power maximization. According to (6), wideband CBF can be converted into multiple narrowband CBF operations using DFT. To simplify the exposition in this subsection, we assume that the array shape is linear ($A = 0$) and the array amplitude response is consistent ($\sigma_\alpha^2 = 0$). Note that our approach still performs well if both of the two assumptions do not hold. This analysis is presented by first considering a single source and focusing only on the signal component. CBF beam power, as a function of the steering angle ϑ, is given

by

$$\begin{aligned} &P(\vartheta, f_n) \\ &= \left|\mathbf{w}^H(\vartheta, f_n)\,\mathbf{a}(\vartheta_k, f_n)\,S_k(f_n)\right|^2 \\ &= |S_k(f_n)|^2 \left|\frac{\sin\left[M\pi(\cos\vartheta - \cos\vartheta_k) f_n/(2f_0)\right]}{M\sin\left[\pi(\cos\vartheta - \cos\vartheta_k) f_n/(2f_0)\right]}\right|^2, \end{aligned} \tag{8}$$

where $\mathbf{w}(\vartheta, f_n) = [w_1, \ldots, w_M]^T \in \mathbb{C}^{M\times 1}$ represents the steering vector and $w_m = \left(1/M\right) e^{-j2\pi f_n (m-1) d\cos(\vartheta)/c}$, $\mathbf{a}(\vartheta_k, f_n) = \left[e^{-j2\pi f_n \tau_{1,k}}, \ldots, e^{-j2\pi f_n \tau_{M,k}}\right]^T \in \mathbb{C}^{M\times 1}$ denotes the array manifold vector for the signal incident from the direction of ϑ_k, and $f_0 = c/(2d)$ is a reference frequency, respectively. When the steering angle ϑ is close to the signal direction ϑ_k, $(\cos\vartheta - \cos\vartheta_k) \approx 0$. Making use of the L'Hospital's rule and Taylor series expansion, (8) can be rewritten as

$$\begin{aligned} &P(\vartheta, f_n) \\ &\approx |S_k(f_n)|^2 \left|\frac{\sin\left[M\pi(\cos\vartheta - \cos\vartheta_k) f_n/(2f_0)\right]}{M\pi(\cos\vartheta - \cos\vartheta_k) f_n/(2f_0)}\right|^2 \\ &= |S_k(f_n)|^2 \left[1 - \frac{[\varphi_k f_n/(2f_0)]^2}{3!} + o\left([\varphi_k f_n/(2f_0)]^2\right)\right]^2 \\ &\approx |S_k(f_n)|^2 \left[1 - \frac{(f_n/f_0)^2}{12}\varphi_k^2\right], \end{aligned} \tag{9}$$

where $o\left([\varphi_k f_n/(2f_0)]^2\right)$ represents the higher-order infinitesimal of $[\varphi_k f_n/(2f_0)]^2$ and $\varphi_k = M\pi(\cos\vartheta - \cos\vartheta_k)$. For the wideband signal, the beam power around ϑ_k is given by

$$\begin{aligned} P(\vartheta) &= \sum_{n=n_l}^{n_h} P(\vartheta, f_n) \\ &\approx \sum_{n=n_l}^{n_h} |S_k(f_n)|^2 \left[1 - \frac{(f_n/f_0)^2}{12}\varphi_k^2\right] \\ &= a_k\left(1 - b_k\varphi_k^2\right), \end{aligned} \tag{10}$$

where $n_l = \text{int}\left(f_l N/f_s + 1\right)$ and $n_h = \text{int}\left(f_h N/f_s + 1\right)$ respectively represent the discrete frequency indices corresponding to f_l and f_h,

$$\begin{aligned} a_k &= \sum_{n=n_l}^{n_h} |S_k(f_n)|^2, \\ b_k &= \frac{\sum_{n=n_l}^{n_h} |S_k(f_n)|^2 (f_n/f_0)^2}{12 a_k}. \end{aligned}$$

Equation (10) suggests that the beam power around ϑ_k is a function of the signal DOA, which satisfies a parabolic model. The maximum of the beam power occurs at the parabola vertex defined by $\varphi_k = 0$ (i.e., $\cos\vartheta = \cos\vartheta_k$), which can be used to acquire the signal DOA as follows

$$\hat{\vartheta}_k = \arg\max_{0\le\vartheta\le\pi} P(\vartheta). \tag{11}$$

An exhaustive search can be avoided by obtaining the signal DOA as the vertex of a parabola fitted through three samples around the beam power peak, which is termed three-point beam power maximization [41]. Sample the beam power at equal cosine interval and denote the sample sequence as $\mathbf{p} = [P(\theta_1), \ldots, P(\theta_L)]$, where $\boldsymbol{\Theta} = [\theta_1, \ldots, \theta_L]$ is a vector consisting of L candidate directions. The angle of the lth candidate direction is given by

$$\theta_l = \arccos\left[1 - (l-1)\,\Delta_\beta\right], \quad l = 1, \ldots, L, \tag{12}$$

where $\Delta_\beta = 2/(L-1)$ is the cosine interval between adjacent samples. Locate the maximum of the sample sequence as $\theta_{l_0} = \underset{\theta_l\in\boldsymbol{\Theta}}{\text{argmax}}\, P(\theta_l)$. Take the cosines of the candidate directions as abscissa of the sample sequence, and denote the three samples around beam power peak as follows

$$\begin{cases} (\beta_1, P_1) = \left(\cos\theta_{l_0-1}, P\left(\theta_{l_0-1}\right)\right) \\ (\beta_2, P_2) = \left(\cos\theta_{l_0}, P\left(\theta_{l_0}\right)\right) \\ (\beta_3, P_3) = \left(\cos\theta_{l_0+1}, P\left(\theta_{l_0+1}\right)\right). \end{cases} \tag{13}$$

DOA estimation exploiting three-point beam power maximization can be straightforwardly obtained by [42]

$$\hat{\vartheta}_k = \arccos\left[\frac{1}{2}\frac{\beta_3^2(P_1 - P_2) + \beta_2^2(P_3 - P_1) + \beta_1^2(P_2 - P_3)}{\beta_3(P_1 - P_2) + \beta_2(P_3 - P_1) + \beta_1(P_2 - P_3)}\right]. \tag{14}$$

Simulation results have shown that, for the single-source scenario, DOA estimation based on beam power maximization can achieve the performance close to CRLB, when the array shape is distortionless. Moreover, this method has strong robustness against array shape distortion and array amplitude response inconsistency.

For the multi-source scenario, without loss of generality, we consider $K = 2$ and the target and interference signals impinge on the array from the directions of ϑ_1 and ϑ_2, respectively. The SIR is defined as the power ratio of the target signal to the interference signal in the analysis frequency band $[f_l, f_h]$, which is given by

$$\text{SIR} = \frac{\sum_{n=n_l}^{n_h} |S_1(f_n)|^2}{\sum_{n=n_l}^{n_h} |S_2(f_n)|^2}. \tag{15}$$

Since the signals from different sources are assumed to be uncorrelated, the beam power of signals from multiple sources can be expressed as the sum of beam power of the signal from individual sources [7]. The beam power around ϑ_1 is given by

$$\begin{aligned} &P(\vartheta) \\ &= \sum_{n=n_l}^{n_h} \left|\mathbf{w}^H(\vartheta, f_n)\left[\sum_{k=1}^{K} \mathbf{a}(\vartheta_k, f_n)\,S_k(f_n)\right]\right|^2 \\ &\approx a_1\left(1 - b_1\varphi_1^2\right) \\ &\quad + \sum_{n=n_l}^{n_h} |S_2(f_n)|^2 \left|\frac{\sin\left[M\pi(\cos\vartheta - \cos\vartheta_2) f_n/(2f_0)\right]}{M\sin\left[\pi(\cos\vartheta - \cos\vartheta_2) f_n/(2f_0)\right]}\right|^2. \end{aligned} \tag{16}$$

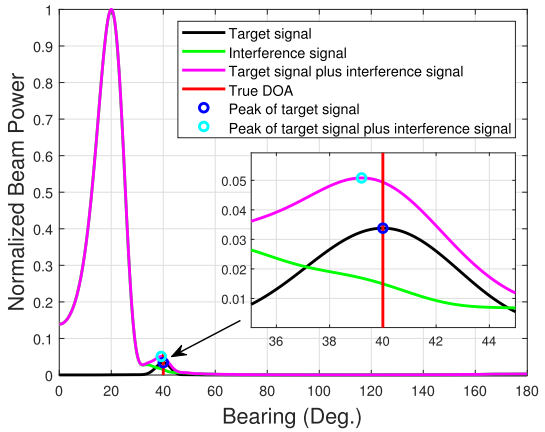

FIGURE 2. Performance degradation caused by energy leakage in a multi-source environment. The DOAs of the target and interference signals are respectively $\vartheta_1 = 40°$ and $\vartheta_2 = 20°$, SIR $= -15$ dB, $M = 32$, $d = 0.8$ m, $c = 1500$ m/s, $f_s = 20$ kHz, $N = 20000$, $f_l = 468.75$ Hz and $f_h = 937.5$ Hz.

It is evident from this expression that the beam power around ϑ_1 is a superposition of the peak beam power of the target signal and energy leaking from the interference beam to the target beam. The leaked energy, resulting from wide beams and high-level sidelobes of CBF, can pollute or even mask the beam power peak of target signal. The magnitude of this effect depends on the bearing of the target signal, the SIR, and the bearing separation between target and interference signals. If one ignores the energy leakage and still calculates the beam power based on element-space data consisting of signals from multiple sources, the performance of DOA estimation based on beam power maximization degrades significantly.

The impact of energy leakage on DOA estimation performance is illustrated in Fig. 2. It is evident that the abscissa of the beam power peak, calculated using element-space data consisting of only the target signal component, corresponds well with the true target bearing. In contrast, the abscissa calculated using data consisting of both the target and interference signals exhibits a noticeable deviation from the true target bearing.

III. ESDR-BASED WIDEBAND DOA ESTIMATION IN A MULTI-SOURCE ENVIRONMENT

As discussed in Section II-B, in the case of a single source, DOA estimation based on beam power maximization can achieve performance close to CRLB. However, in the presence of multiple sources, its performance is severely affected by the energy leaking from the interference beam to the target beam. This motivates us to reconstruct the element-space data with respect to the SOI, to approach the received hydrophone data of the single-source scenario, thus completely eliminating or significantly reducing the unacceptable energy leakage. Therefore, in this paper, we propose a robust ESDR-based wideband DOA estimation method to acquire the accurate bearings of the weak signals in a multi-source environment.

In this section, we firstly introduce the ESDR based on the ISF technique, and then develop a data-driven algorithm to adaptively obtain the ISF parameter of each signal, including received signal waveform, time-delay, and amplitude correction factor. Finally, we present the ESDR-based wideband DOA estimation method, which consists of two stages: 1) sequential detection and coarse estimation, and 2) fine estimation.

A. ESDR USING THE ISF TECHNIQUE

ESDR can be achieved using an ISF technique that removes the element-space waveforms of all the signals, excepting the one currently interested, from the received hydrophone data. ESDR for the kth signal can be expressed as

$$\begin{aligned} r_{m,k}(t) &= r_m(t) - \sum_{i=1, i\neq k}^{K} \hat{\eta}_m \hat{h}_i\left(t - \hat{\tau}_{m,i}\right) \\ &= \alpha_m\left[s_k\left(t - \tau_{m,k}\right) + v_m(t)\right] \\ &\quad + \sum_{i=1, i\neq k}^{K}\left[\alpha_m s_i\left(t - \tau_{m,i}\right) - \hat{\eta}_m \hat{h}_i\left(t - \hat{\tau}_{m,i}\right)\right], \end{aligned} \tag{17}$$

where $\hat{h}_i(t)$ represents the estimate of the received signal waveform of the ith signal (The term $h_i(t)$ is notated to distinguish the received signal waveform from the signal waveform $s_i(t)$), $\hat{\tau}_{m,i}$ denotes the estimate of time-delay for the ith signal when propagation from the reference hydrophone to the mth hydrophone, and η_m is an amplitude correction factor defined as the amplitude ratio of the ith signal component received at the mth hydrophone to that in $\hat{h}_i(t)$, i.e.,

$$\hat{\eta}_m = \frac{\alpha_m}{\alpha}, \quad m = 1, \ldots, M, \tag{18}$$

where α represents the scale factor of $s_i(t)$ in $\hat{h}_i(t)$. The received signal waveform $h_i(t)$, time-delay $\tau_{m,i}$, and amplitude correction factor η_m are collectively termed the ISF parameters of the ith signal. The combination $\hat{h}_{m,i}(t) = \hat{\eta}_m \hat{h}_i\left(t - \hat{\tau}_{m,i}\right)$ provides an estimation of the element-space waveform for the ith signal component received at the mth hydrophone.

It is worth noting that the first term on the second line of (17) represents received hydrophone data in a single-source scenario containing only the SOI. The second term denotes the sum of element-space waveform estimation errors of all other signals. Hence, the reconstructed element-space data can be considered the sum of received hydrophone data in a single-source scenario and element-space waveform estimation errors of all the interference signals. As indicated by this expression, the effect of ESDR depends on the estimation accuracy of ISF parameters. If these parameters are estimated accurately enough, the element-space waveforms of all the interference signals can be either completely eliminated or significantly reduced, generating element-space data comparable to the received hydrophone data of a single-source scenario.

According to the data model discussed in Section II-A, the estimate of the received signal waveform exploiting CBF can be expressed as

$$\hat{h}_i(t) = \frac{1}{M}\sum_{m=1}^{M} r_m\left(t + \hat{\tau}_{m,i}\right). \tag{19}$$

The corresponding estimate of time-delay can be given by

$$\hat{\tau}_{m,i} = \frac{x_m \cos\hat{\vartheta}_i - y_m \sin\hat{\vartheta}_i}{c}, \tag{20}$$

where $\hat{\vartheta}_i$ represents the estimate of DOA of the ith signal. If the time-delay is estimated accurately, the estimate of the received signal waveform $\hat{h}_i(t)$ can be approximated as a coherent sum of the ith signal component from various hydrophones. Thus, the scale factor of $s_i(t)$ in $\hat{h}_i(t)$ is given by $\alpha = \frac{1}{M}\sum_{m=1}^{M}\alpha_m$. The estimate of the amplitude correction factor can be given by

$$\hat{\eta}_m = \frac{\alpha_m}{\frac{1}{M}\sum_{m=1}^{M}\alpha_m} = \frac{\alpha_m}{\mu_\alpha}. \tag{21}$$

It is worth noting that $\hat{\eta}_m$ can be considered the relative amplitude response of the mth hydrophone, i.e., the ratio of the mth amplitude response coefficient to the mean coefficient.

It is evident from (20) and (21) that the exact coordinates and amplitude response coefficient of each hydrophone of the array are required to estimate the ISF parameters accurately, which is difficult for a distorted towed array. For a linear array ($A = 0$) with consistent array amplitude response ($\sigma_\alpha^2 = 0$), the estimations of time-delay and amplitude correction factor are respectively simplified as

$$\hat{\tau}_{m,i} = \frac{(m-1)d\cos\hat{\vartheta}_i}{c} \tag{22}$$

and

$$\hat{\eta}_m = \frac{\alpha_m}{\mu_\alpha} = 1. \tag{23}$$

As indicated by these expressions, the exact coordinates and amplitude response coefficient are no longer necessary for estimations in this case. However, assumptions of the linear array shape and consistent array amplitude response frequently mismatch those of the real towed array, as discussed in Section II-A. If one ignores these mismatches and still estimates the ISF parameters using (19), (22), and (23), the estimation accuracies decrease greatly. Thus, the element-space waveforms of interference signals are not properly removed, which can seriously degrade the ESDR accuracy. Hence, a suitable algorithm is needed to acquire the accurate ISF parameters without requiring the exact knowledge of the hydrophone coordinates and amplitude response coefficients.

B. ITERATIVE ALGORITHM FOR ISF PARAMETER ESTIMATION

In this subsection, an iterative algorithm, which is robust to array shape distortion and array amplitude response inconsistency, is developed to adaptively obtain the accurate ISF parameters. In the rest of this paper, unless otherwise stated, the hydrophone coordinates (x_m, y_m) and relative amplitude response η_m, obtained based on the assumptions of linear array shape and consistent array amplitude response, are termed nominal array configuration. The iterative algorithm for ISF parameter estimation is described as follows.

Step 0: Obtain the initial estimates of time-delay $\hat{\tau}_{m,i}^{(0)}$ and the received signal waveform $\hat{h}_i^{(0)}(t)$ based on the nominal array configuration, according to (22) and (19).

Step q: $q = 1, 2, \ldots, Q$

1) Calculate the correlation function between element-space data at the mth hydrophone and the estimated received signal waveform of the ith signal as follows:

$$R_m(u) = \int_0^T r_m(t+u)\,\hat{h}_i^{(q-1)}(t)dt, \quad -\tau_{\max} \le u \le \tau_{\max}, \tag{24}$$

where $\tau_{\max} = (M-1)\,d/c$ represents the boundary value of time-delay searching range.

2) Locate the maximum of $R_m(u)$ as

$$u_m^{(q)} = \underset{-\tau_{\max}\le u\le\tau_{\max}}{\operatorname{argmax}} R_m(u), \tag{25}$$

and denote this maximum as $p_m^{(q)} = R_m\left(u_m^{(q)}\right)$. The estimate of time-delay is then given by

$$\hat{\tau}_{m,i}^{(q)} = u_m^{(q)} - u_1^{(q)}, m = 1, \ldots, M. \tag{26}$$

3) Perform the enhanced beamforming using the renewed estimate of time-delay and update the estimate of the received signal waveform with the obtained values

$$\hat{h}_i^{(q)}(t) = \frac{1}{M}\sum_{m=1}^{M} r_m\left(t + \hat{\tau}_{m,i}^{(q)}\right). \tag{27}$$

These three substeps are carried on till the following termination rule

$$\hat{q} = \min_q \left\{ q : \sqrt{\frac{1}{M}\sum_{m=1}^{M}\left|\hat{\tau}_{m,i}^{(q)} - \hat{\tau}_{m,i}^{(q-1)}\right|^2} \le \varepsilon,\ q \ge Q \right\} \tag{28}$$

is satisfied, where $\Delta\tau = \sqrt{\frac{1}{M}\sum_{m=1}^{M}\left|\hat{\tau}_{m,i}^{(q)} - \hat{\tau}_{m,i}^{(q-1)}\right|^2}$ is the iteration termination indicator (ITI) used to evaluate the variation of the estimated time-delay between adjacent iterations. The terms $\varepsilon > 0$ and $Q \ge 1$ are set in advance and the settings are discussed in Section IV-A. Simulations in the sequel confirm the fast convergence property and robustness of this algorithm.

In step 0 of this algorithm, the value of $\hat{\vartheta}_i$ in (22) is determined exploiting the three-point beam power maximization (Eq. (14)), and the time-delay estimation is conducted based on the hypothetical linear array shape. However, in the qth step, a data-driven time-delay estimation is obtained from the relative position offset of correlation peaks. Note that the

estimate of the received signal waveform $\hat{h}_i^{(q)}(t)$ serves as the reference signal used in correlation calculation, rather than element-space data of the reference hydrophone $r_1(t)$. This is because the estimated received signal waveform exhibits a higher signal-to-interference-plus-noise ratio (SINR) owing to the array gain provided by beamforming. Furthermore, the estimated received signal waveform can simultaneously be served as adaptive iterative feedback. It is evident from (27) that the improvement in time-delay estimation accuracy increases the SINR of the estimated received signal waveform. This updated estimate of received signal waveform is then used for time-delay estimation in the next iteration to further improve the estimation accuracy.

At the conclusion of an iteration, the estimate of time-delay $\hat{\tau}_{m,i}^{(\hat{q})}$ is considered to be approximately compliant with the true time-delay, which is a function of hydrophone coordinates and the DOA of the signal. The estimate of the received signal waveform $\hat{h}_i^{(\hat{q})}(t)$ can then be approximated as a coherent sum of the ith signal component from various hydrophones, i.e.,

$$\hat{h}_i^{(\hat{q})}(t) \approx \frac{\sum_{m=1}^{M}\alpha_m}{M}s_i(t)+\frac{1}{M}\sum_{m=1}^{M}\alpha_m v_m\left(t+\hat{\tau}_{m,i}^{(\hat{q})}\right). \quad (29)$$

Substituting (3) and (29) into (24) yields the amplitude of the mth correlation peak

$$\begin{aligned} p_m^{(\hat{q})} &= \int_0^T r_m\left(t+\hat{\tau}_{m,i}^{(\hat{q})}\right)\hat{h}_i^{(\hat{q})}(t)dt \\ &\approx \alpha_m\frac{\sum_{m=1}^{M}\alpha_m}{M}\int_0^T s_i^2(t)dt+\frac{\alpha_m^2}{M}\int_0^T v_m^2(t)dt \\ &= a_m\mu_a E_{s_i}+\frac{\alpha_m^2}{M}\sigma_{v_m}^2, \end{aligned} \quad (30)$$

where $E_{s_i}=\int_0^T s_i^2(t)dt$ represents the energy of the ith signal and $E_{v_m}=\int_0^T v_m^2(t)dt$ denotes the energy of noise at the mth hydrophone, respectively. In (30), we assume that the noises at different hydrophones are incoherent with each other. if $E_{s_i}\gg E_{v_m}/M$, then $p_m^{(\hat{q})}$ can be approximated as

$$p_m^{(\hat{q})} \approx a_m\mu_\alpha E_{s_i}. \quad (31)$$

Substituting (31) into (21) yields the estimate of amplitude correction factor

$$\begin{aligned} \hat{\eta}_m &= \frac{\alpha_m}{\frac{1}{M}\sum_{m=1}^{M}\alpha_m} \\ &= \frac{\alpha_m\mu_\alpha E_{s_i}}{\frac{1}{M}\sum_{m=1}^{M}\alpha_m\mu_\alpha E_{s_i}} \\ &\approx \frac{p_m^{(\hat{q})}}{\frac{1}{M}\sum_{m=1}^{M}p_m^{(\hat{q})}}. \end{aligned} \quad (32)$$

It can be seen from this expression that the ratio of the mth correlation peak amplitude to the mean amplitude provides an estimation for η_m.

This approach is summarized in Algorithm 1. Its convergence property and robustness are verified by simulations in Section IV-A.

Algorithm 1 Iterative Algorithm for Robust ISF Parameter Estimation

Input: $r_m(t)$: The element-space data.
$\hat{\vartheta}_i$: The pre-estimated DOA of the ith signal.

Set $q=0$. Obtain the initial estimates of time-delay $\hat{\tau}_{m,i}^{(0)}$ and received signal waveform $\hat{h}_i^{(0)}(t)$ based on hypothetical linear array shape, according to (22) and (19).

repeat

1) $q=q+1$.
2) Calculate the correlation function $R_m(u)$ between element-space data at the mth hydrophone $r_m(t)$ and the estimate of the received signal waveform $\hat{h}_i^{(q-1)}$ according to (24).
3) Determine the position $u_m^{(q)}$ and amplitude $p_m^{(q)}$ of the maximal correlation peak and estimate the time-delay $\hat{\tau}_{m,i}^{(q)}$ according to (26).
4) Perform the enhanced beamforming using the renewed time-delay $\hat{\tau}_{m,i}^{(q)}$ and update the estimate of the received signal waveform $\hat{h}_i^{(q)}(t)$, according to (27).

until $\Delta\tau\le\varepsilon$ or $q\ge Q$.

Set $\hat{q}=q$. Let $\hat{h}_i(t)=\hat{h}_i^{(\hat{q})}(t)$, $\hat{\tau}_{m,i}=\hat{\tau}_{m,i}^{(\hat{q})}$, and the $\hat{\eta}_m$ is obtained according to (32).

Output: $\left\{\hat{h}_i(t),\hat{\tau}_{m,i},\hat{\eta}_m\right\}$: The estimate of ISF parameters of the ith signal.

It is worth noting that the ISF parameter estimation of different signals affects each other in a multi-source environment. Therefore, a suitable operation procedure is required to mitigate this influence. The corresponding process presented in this paper includes two stages: 1) sequential detection and coarse estimation, 2) fine estimation. The two stages are discussed in detail below.

C. SEQUENTIAL DETECTION AND COARSE ESTIMATION

In the presence of multiple sources, the estimation accuracy of the DOA and ISF parameters of the weak signals is affected by the strong signal, particularly when the strength of the strong signal is much larger than that of the weaker ones. Hence, a technique termed sequential detection is presented below to mitigate this influence and obtain the coarse estimates of DOA and ISF parameters for each detected signal.

First, set $r_m^*(t)=r_m(t)$ and calculate the sample sequence of beam power utilizing $r_m^*(t)$. Signal detection from sample sequence begins with the strongest one. After that signal component is located and its coarse DOA estimation $\hat{\theta}_k^c$ (The superscript c denotes coarse) is obtained using three-point

beam power maximization, we remove it from $r_m^*(t)$ exploiting an ISF technique with the following three steps.

1) Estimate the ISF parameters of the kth signal, i.e., the received signal waveform $\hat{h}_k^c(t)$, time-delay $\hat{\tau}_{m,k}^c$, and amplitude correction factor $\hat{\eta}_m^c$, using $r_m^*(t)$ and $\hat{\theta}_k^c$, according to Algorithm 1.
2) Remove the kth signal component from $r_m^*(t)$ utilizing the ISF technique as follows:

$$r_m^*(t) = r_m^*(t) - \hat{\eta}_m^c \hat{h}_k^c\left(t - \hat{\tau}_{m,k}^c\right), \quad m = 1, \ldots, M. \tag{33}$$

3) Calculate the sample sequence of the beam power exploiting the updated element-space data $r_m^*(t)$.

Steps 1-3 are repeated until the updated sample sequence does not contain any peaks that can be associated with the signals. After each signal is removed, the maximal value of the updated sample sequence is compared with a predefined threshold T_{th}. If this maximal value exceeds the threshold, an additional signal is assumed to be exist in the remaining element-space data and the procedure is repeated. The detection threshold T_{th} is assumed to be known in advance. (The determination of T_{th} involves the selection of detector and false alarm probability (PFA), which is discussed in [43], [44]).

D. FINE ESTIMATION

Once the sequential detection is finished, the coarse estimates of DOA and ISF parameters of all the detected signals are obtained, i.e., $\left\{\hat{\theta}_k^c, \hat{h}_k^c(t), \hat{\tau}_{m,k}^c, \hat{\eta}_m^c\right\}, k = 1, 2, \ldots, \hat{K}$, where $\hat{K}$ is the number of detected signals. In order to further mitigate the influence of other signals on the one currently concerned, we reconstruct the element-space data to approach the received hydrophone data of a single-source scenario. A refined estimate of DOA can then be acquired from the reconstructed data. The fine estimation is performed as follows. 1)

1) Set $\hat{\theta}_k^r = \hat{\theta}_k^c$, $\hat{h}_k^r(t) = \hat{h}_k^c(t)$, $\hat{\tau}_{m,k}^r = \hat{\tau}_{m,k}^c$, $\hat{\eta}_m^r = \hat{\eta}_m^c$, and $k \in \left\{1, 2, \ldots, \hat{K}\right\}$ (The superscript r denotes refined).
2) For $k = 1 \to \hat{K}$, do
   a) Reconstruct element-space data for the kth signal by removing the element-space waveforms of all other detected signals from the received hydrophone data

$$\hat{r}_{m,k}(t) = r_m(t) - \sum_{i=1, i\neq k}^{\hat{K}} \hat{\eta}_m^r h_i^r\left(t - \hat{\tau}_{m,i}^r\right), \quad m = 1, \ldots, M. \tag{34}$$

   b) Refine the DOA estimation of the kth signal exploiting reconstructed element-space data $\hat{r}_{m,k}(t)$ and update $\hat{\theta}_k^r$ with the resulting value.
   c) Refine the ISF parameter estimation of the kth signal using $\hat{r}_{m,k}(t)$ and $\hat{\theta}_k^r$ according to Algorithm 1, and update $\hat{h}_k^r(t)$, $\hat{\tau}_{m,k}^r$, and $\hat{\eta}_m^r$ with the obtained values.

It is worth noting that, during the sequential detection, ISF parameter estimation for previously detected strong signals is also affected by subsequently detected weaker ones, particularly when their strengths are comparable or the bearing separation is small. To mitigate this influence, ISF parameter estimation for the current signal is performed again utilizing reconstructed element-space data and the refined estimate of DOA. The updated ISF parameters are then used to improve the ESDR of subsequent weaker signals.

Algorithms described in Sections III-B, III-C, and III-D are combined into an integral algorithm and presented in Algorithm 2, which is given at the upper left of the next page.

E. CALCULATION COMPLEXITY

In complexity analysis, we neglect all operations whose calculation complexity not depending on MN. We can conclude from the proposed algorithm that the stage of sequential detection and coarse estimation requires the calculation of $\hat{K}+1$ beam power sample sequences (consisting of L candidate directions), $\hat{K}$ ISF parameters estimations (Algorithm 1), and $\hat{K}$ interference signal removals from the element-space data (Eq. (33)). The stage of fine estimation requires the calculation of $\hat{K}$ ESDRs (Eq. (34) and consisting of $\hat{K}-1$ signal removals), $3\hat{K}$ beam power samples (three-point beam power maximization), and $\hat{K}$ ISF parameters estimations. For the ISF parameters estimation, it requires the calculation of Q cross-correlations between tracking beam data and every element-space data (Eq. (24)) and $Q+1$ time-domain beamforming (Eq. (27)). In total, the proposed algorithm involves the calculation of $L(\hat{K}+1)+3\hat{K}$ beam power samples, $2\hat{K}Q$ cross-correlations, $2\hat{K}(Q+1)$ time-domain beamforming, and $\hat{K}^2$ interference signal removals.

The calculation of the beam power samples is conducted in the frequency domain and M N-samples DFTs are required for each stage. Besides, the number of frequency bins used for beam power calculation is $N_{fb} = n_h - n_l + 1$. For the cross-correlation between tracking beam data and every element-space data, it requires the calculation of $2M + 1$ $2N$-samples DFTs. For both time-domain beamforming and signal removal, an N_{fo} order fractional time-delay filter is utilized to achieve the precise time-delay. The DFT is achieved by the efficient Fast Fourier Transform (FFT). Thus, the calculation of M N-samples DFT takes $MN\log_2 N$ complex multiplications and additions. For the calculation of each beam power sample, it takes MN_{fb} complex multiplications and $(M-1)N_{fb}$ complex additions. For the calculation of cross-correlation, it takes $4(2M+1)N\log_2 N$ complex multiplications and additions. For the calculation of time-domain beamforming, it takes $(N_{fo}+1)MN$ real multiplications and $N_{fo}MN+(M-1)N$ real additions. For the calculation of

Algorithm 2 Robust ESDR-Based Wideband DOA Estimation Algorithm

Input: $r_m(t)$: Received hydrophone data defined by (3).

Sequential Detection and Coarse Estimation

Set $k=0$ and $r_m^*(t)=r_m(t)$. Calculate the sample sequence of beam power $\mathbf{p}=[P(\theta_1),\cdots,P(\theta_L)]$ utilizing $r_m^*(t)$, and locate its maximum as $\theta_{l_0}=\underset{\theta_l\in\boldsymbol{\Theta}}{\operatorname{argmax}}\,P(\theta_l)$.

while $P\left(\theta_{l_0}\right)>T_{th}$ **do**

1) $k=k+1$.
2) Estimate the DOA of the kth signal $\hat{\theta}_k^c$ using the three-point beam power maximization, according to (14).
3) Estimate the ISF parameters of the kth signal utilizing $r_m^*(t)$ and $\hat{\theta}_k^c$, according to Algorithm 1.
4) Remove the kth signal component from $r_m^*(t)$ exploiting the ISF technique, according to (33).
5) Calculate $\mathbf{p}$ using the updated $r_m^*(t)$ and locate its maximum as $\theta_{l_0}=\underset{\theta_l\in\boldsymbol{\Theta}}{\operatorname{argmax}}\,P(\theta_l)$.

end while

$\hat{K}=k$: The number of detected signals.

$\left\{\hat{\theta}_k^c,\hat{h}_k^c(t),\hat{\tau}_{m,k}^c,\hat{\eta}_m^c\right\}_{k=1}^{\hat{K}}$: The coarse estimates of DOA and ISF parameters of all the detected signals.

Fine Estimation

Set $\hat{\theta}_k^r=\hat{\theta}_k^c$, $\hat{h}_k^r(t)=\hat{h}_k^c(t)$, $\hat{\tau}_{m,k}^r=\hat{\tau}_{m,k}^c$, $\hat{\eta}_m^r=\hat{\eta}_m^c$, and $k\in\left\{1,\cdots,\hat{K}\right\}$.

for $k=1\rightarrow\hat{K}$ **do**

1) Reconstruct element-space data for the kth signal using $\left\{\hat{h}_i^r(t),\hat{\tau}_{m,i}^r,\hat{\eta}_m^r\right\}_{i=1,i\neq k}^{\hat{K}}$ according to (34).
2) Refine and update the DOA estimation of the kth signal employing reconstructed element-space data.
3) Refine and update the ISF parameter estimation of the kth signal utilizing reconstructed element-space data and the refined estimate of DOA, according to Algorithm 1.

end for

Output: $\hat{\theta}_k^r,k\in\left\{1,\cdots,\hat{K}\right\}$: Refined estimate of DOA.

signal removal, it takes $\left(N_{fo}+2\right)MN$ real multiplications and $\left(N_{fo}+1\right)MN$ real additions.

The complex multiplication can be obtained by four real multiplications and two real additions, and the complex addition requires two real additions [42]. Therefore, the overall calculation complexity of the proposed algorithm is $\left[2\hat{K}(Q+1)\left(N_{fo}+1\right)+\hat{K}^2\left(N_{fo}+2\right)+8\log_2 N+64\hat{K}Q\log_2 N\right]MN+4\left[L\left(\hat{K}+1\right)+3\hat{K}\right]MN_{fb}$ real multiplications and $\left[2\hat{K}(Q+1)\left(N_{fo}+1\right)+\hat{K}^2\left(N_{fo}+1\right)+8\log_2 N+64\hat{K}Q\log_2 N\right]MN+4\left[L\left(\hat{K}+1\right)+3\hat{K}\right]MN_{fb}$ real additions. Since $\hat{K}$, Q, and N_{fo} are all far less than N, we may conclude that the algorithm complexity is $O\left(\hat{K}QMN\log_2 N\right)$ operations, where $O(\cdot)$ denotes big O notation. It is observed that the computational load mainly lies in the calculation of beam power sample and cross-correlation, and both of them can be achieved by the efficient FFT. Besides, the proposed method can simultaneously obtain DOAs and tracking beam data of $\hat{K}$ sources.

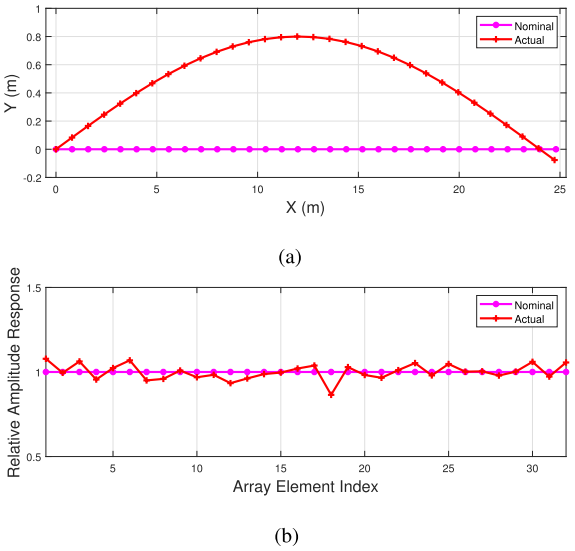

FIGURE 3. Nominal and actual array configuration of a distorted towed array. (a) Hydrophone coordinates. (b) Relative amplitude response coefficients.

IV. NUMERICAL SIMULATIONS

In this section, we firstly analyze the convergence property and robustness of the iterative algorithm for ISF parameter estimation. Then we investigate the impact of SIR, bearing separation (between the target and interference signals), and SNR on the DOA estimation performance of the proposed method, respectively.

Suppose that the data is collected from a distorted towed array comprising of $M=32$ elements with inter-element spacing $d=0.8$ m. The parameters for describing array shape distortion are set to be $A=0.8$ and $g=\pi/24$, respectively. The actual values of the hydrophone coordinates are shown in Fig. 3(a) and compared with the nominal values. The fluctuation of the amplitude response coefficients of this array is set to be $\sigma_\alpha/u_\alpha=0.04$. The actual values of the relative amplitude response (i.e., $\alpha_m/\mu_\alpha, m=1,\ldots,M$) are shown in Fig. 3(b) and compared with the nominal values. The sound velocity is set to be 1500 m/s. The time analysis window length is $T=1$ s and the sampling rate is $f_s=20$ kHz. Thus, the sampling number is $N=20000$ and the sampling interval is $\mathrm{T_s}=50\,\mu$s. The lower and upper bounds of the analysis frequency band are set to be $f_l=468.75$ Hz and $f_h=937.5$ Hz, respectively. The influence of off-grid on the performance of the proposed method decreases as

the number of candidate directions increases. However, the calculation complexity of the proposed method is proportional to the number of candidate directions. To balance the DOA estimation performance and the calculation complexity, we set the number of candidate directions to be $L = 2M + 1$. In this case, all of the three samples around the beam power peak are within the half-power width (3 dB width) of the main beam, which can satisfy the essential requirement of DOA estimation exploiting three-point beam power maximization, and the influence of off-grid is reduced to an acceptable level. The input SNR of the kth signal is defined as the power ratio of signal to noise in the analysis frequency band $[f_l, f_h]$, which is given by

$$SNR_k = \frac{\sum_{n=n_l}^{n_h} |S_k(f_n)|^2}{\sum_{n=n_l}^{n_h} |V(f_n)|^2}. \tag{35}$$

A. PERFORMANCE EVALUATION OF ITERATIVE ALGORITHM FOR ISF PARAMETER ESTIMATION

In this subsection, the convergence property and robustness of the iterative algorithm used for ISF parameter estimation are investigated in detail. A simulation is conducted in which the signal is assumed to be incident on the array from a direction of 60° with SNR= 0 dB. To evaluate the ISF parameter estimation accuracy at the qth iteration, we define the following assessment criteria. The estimation accuracy of the received signal waveform is measured by the correlation coefficient (CC) between the estimated received signal waveform and the true received signal waveform, which is given by

$$CC_{rsw}^{(q)} = \frac{\int_0^T \hat{h}_k^{(q)}(t) h_k(t)\, dt}{\sqrt{\int_0^T \left[\hat{h}_k^{(q)}(t)\right]^2 dt \int_0^T [h_k(t)]^2 dt}}. \tag{36}$$

The estimation accuracies of time-delay and amplitude correction factor are evaluated using the root mean square error (RMSE) of the estimates from M hydrophones, which are respectively given by

$$RMSE_{td}^{(q)} = \sqrt{\frac{1}{M}\sum_{m=1}^{M}\left|\hat{\tau}_{m,k}^{(q)} - \tau_{m,k}\right|^2} \tag{37}$$

and

$$RMSE_{acf}^{(q)} = \sqrt{\frac{1}{M}\sum_{m=1}^{M}\left|\hat{\eta}_m^{(q)} - \eta_m\right|^2}. \tag{38}$$

Fig. 4(a) shows the corresponding variations of the iteration termination indicator, which decreases rapidly and converges to $5.356 * 10^{-8}$ T_s at the seventh iteration. The convergence curves of the ISF parameter estimations corresponding to Fig. 4(a) are shown in Fig. 4(b), 4(c) and 4(d), respectively. The results indicate that the proposed iterative ISF parameter estimation algorithm is convergent. Furthermore, the estimates of the three ISF parameters all converge to the accurate values just at the second iteration. It can be noted that the convergence speeds of the three ISF parameters are

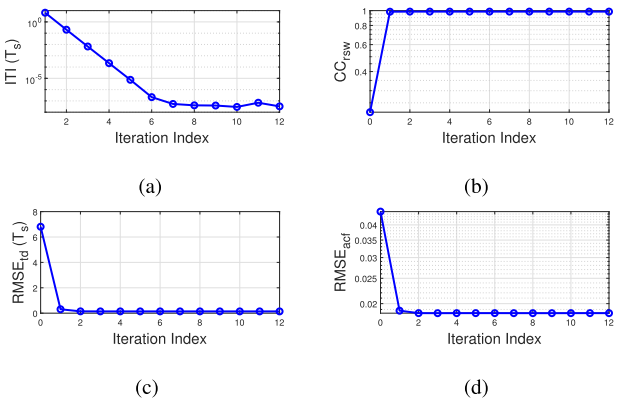

FIGURE 4. Convergence property analysis of the iterative algorithm for ISF parameter estimation. (a) Iteration termination indicator. (b) The correlation coefficient between the estimated received signal waveform and the true received signal waveform. (c) RMSE of time-delay estimation. (d) RMSE of the estimates of amplitude correction factor.

TABLE 1. Estimation accuracy of ISF parameters.

	CC_{rsw}	$RMSE_{td}$ (T_s)	$RMSE_{acf}$
Nominal based	0.217	6.808	0.045
Algorithm 1	0.985	0.144	0.019

faster than that of the iteration termination indicator. This is because the variations of CC_{rsw}, $RMSE_{td}$, and $RMSE_{acf}$ are all reduced to negligible levels when the indicator is below 0.01 T_s. Hence, $\varepsilon = 0.01$ T_s and $Q = 3$ can be specified as the termination criteria and applied to the remaining simulations.

The final estimates of the ISF parameters can be obtained once the iteration terminates. The corresponding accuracy of each parameter is listed in Table 1 and compared with that obtained based on the nominal array configuration. It can be seen that the improvement in estimation accuracy by using Algorithm 1 is evident. This is to be expected since Algorithm 1 is a data-driven method. Thus, the obtained estimates of time-delay are approximately compliant with the actual hydrophone coordinates and signal DOA. Moreover, the updated estimate of the received signal waveform is taken as adaptive iterative feedback and used for time-delay estimation in the next iteration, further improving the estimation accuracy. As discussed in Section III-B, the accurate estimates of the received signal waveform and the amplitude correction factor can then be obtained utilizing the resulting estimates of time-delay. In contrast, the method based on the nominal array configuration is data-independent. Thus, its resulting estimates exhibit significant deviations from the actual values, due to the incorrect assumptions of hydrophone coordinates and amplitude response coefficients. Fig. 5(a) and 5(b) show the time-delay offsets between adjacent hydrophones (i.e., $\Delta\hat{\tau}_{m,k} = \hat{\tau}_{m,k} - \hat{\tau}_{(m-1),k}, m = 2, \ldots, M$) and the amplitude correction factors, respectively. It is evident that both estimates obtained using Algorithm 1 fluctuate around the actual values. However, for the estimates obtained based on nominal array configuration, the time-delay offsets are fixed at $d\cos\hat{\theta}_k/c = 5.354\,T_s$ and the amplitude correction factors are fixed at $\hat{\eta}_m = 1$ for all elements.

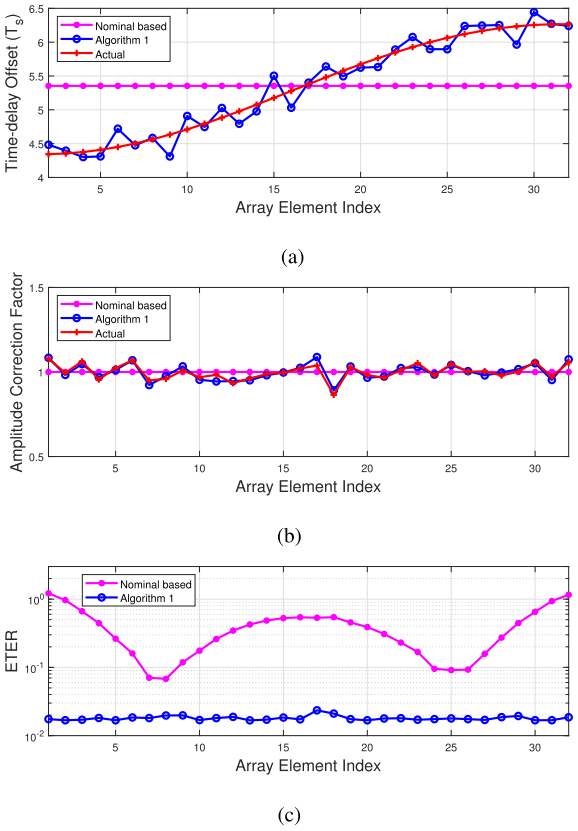

FIGURE 5. ISF parameter estimation results. (a) The estimates of time-delay offsets between adjacent hydrophones. (b) The estimates of the amplitude correction factors. (c) Energy ratios of the element-space waveform estimation errors to the true element-space waveforms.

As discussed in Section III-A, the expression $\hat{h}_{m,k}(t) = \hat{\eta}_m \hat{h}_k\left(t - \hat{\tau}_{m,k}\right)$ provides an estimation of the element-space waveform for the kth signal at the mth hydrophone. The estimation accuracy of the element-space waveform is measured using the energy ratio of estimation error to true element-space waveform (ETER), which is defined as

$$ETER_{m,k} = \frac{\int_0^T \left[\hat{\eta}_m \hat{h}_k\left(t - \hat{\tau}_{m,k}\right) - \alpha_m s_k\left(t - \tau_{m,k}\right)\right]^2 dt}{\int_0^T \left[\alpha_m s_k\left(t - \tau_{m,k}\right)\right]^2 dt} \tag{39}$$

Fig. 5(c) illustrates $ETER_{m,k}$ calculated utilizing the ISF parameters produced by both Algorithm 1 and the method based on nominal array configuration. It is evident that the maximum achieved by Algorithm 1 is less than 0.024, while the minimum achieved by the nominal based method is greater than 0.067. Moreover, the $ETER_{m,k}$ achieved by Algorithm 1 is mostly uniform and almost fixed at 0.02 for $\forall m$. In contrast, the $ETER_{m,k}$ achieved by the nominal based method exhibits a significant fluctuation. This proves that Algorithm 1 provides a practical approach to acquire the accurate estimates of element-space waveforms, without requiring the exact hydrophone coordinates and amplitude response coefficients of the distorted towed array.

Note that the time-delay estimation in Algorithm 1 can be seen as a matching filter (MF), as shown in (24). MF is a popular technique for array signal processing and is widely applied in the active sonar system, where the reference signal (transmitted signal) is known. However, unlike the MF in active sonar, the reference signal (ship-radiated noise) used for MF in passive sonar cannot be accessed directly. Hence, it is necessary to estimate the received signal waveform from the received hydrophone data, which is still an open problem, particularly when the strong interference sources and array shape distortion coexist. The corresponding CRLB of time-delay estimation is given by [45]

$$\mathrm{var}\left(\hat{\tau}\right) \geq \frac{3}{8\pi^2 T} \frac{1 + SNR_k + SNR_k^{ref}}{SNR_k SNR_k^{ref}} \frac{1}{f_2^3 - f_1^3}, \tag{40}$$

where SNR_k^{ref} represents the SNR of the reference signal. As indicated by this expression, for a given SNR_k, the performance of time-delay estimation depends on the SNR_k^{ref}. The higher is the SNR_k^{ref}, the lower the time-delay estimation variance. For Algorithm 1, at the conclusion of an iteration, the estimated received signal waveform (tracking beam data) can be approximated as a coherent sum of the kth signal component from various hydrophones of the array. If the noises at different hydrophones are assumed to be incoherent, the corresponding SNR can be approximated as $SNR_k^{tb} = M \times SNR_k$ (The superscript tb denotes the tracking beam).

We proceed with the simulation to demonstrate the time-delay estimation performance of Algorithm 1, and compare it with the maximum likelihood (ML) method based on the nominal array configuration, the generalized cross-correlation (GCC) based method [46], and the MF based method. The reference signals used in the GCC based method, Algorithm 1, and the MF based method are respectively the element-space data of the reference hydrophone, the estimated received signal waveform, and the actual received signal waveform. Therefore, the MF based method is the upper performance bound of Algorithm 1. According to (40), the corresponding CRLBs are respectively given by

$$\mathrm{var}\left(\hat{\tau}_{GCC}\right) \geq \frac{3}{8\pi^2 T} \frac{2 + 1/SNR_k}{SNR_k} \frac{1}{f_2^3 - f_1^3}, \tag{41}$$

$$\mathrm{var}\left(\hat{\tau}_{\mathrm{Alg1}}\right) \geq \frac{3}{8\pi^2 T} \frac{1 + 1/M + 1/(M \times SNR_k)}{SNR_k} \frac{1}{f_2^3 - f_1^3}, \tag{42}$$

and

$$\mathrm{var}\left(\hat{\tau}_{MF}\right) \geq \frac{3}{8\pi^2 T} \frac{1}{SNR_k} \frac{1}{f_2^3 - f_1^3}. \tag{43}$$

As indicated by these expressions, since $M \gg 1$, the variances of both Algorithm 1 and the MF based algorithm are smaller than that of the GCC based algorithm. Furthermore, the variance of Algorithm 1 is increasingly close to that of the MF based algorithm as the SNR_k increases.

The target signal is assumed to be incident on the array from a direction of 60° with input SNR varies over the interval

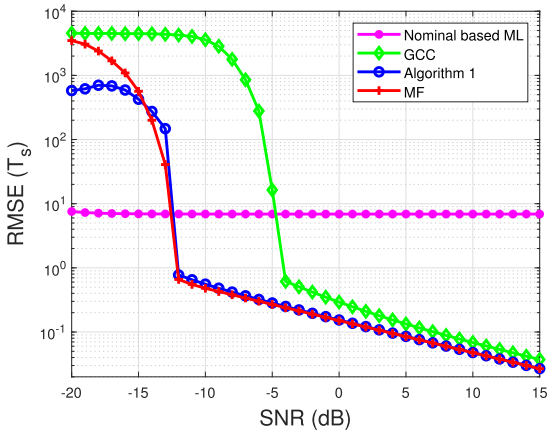

FIGURE 6. RMSE of time-delay estimation versus SNR.

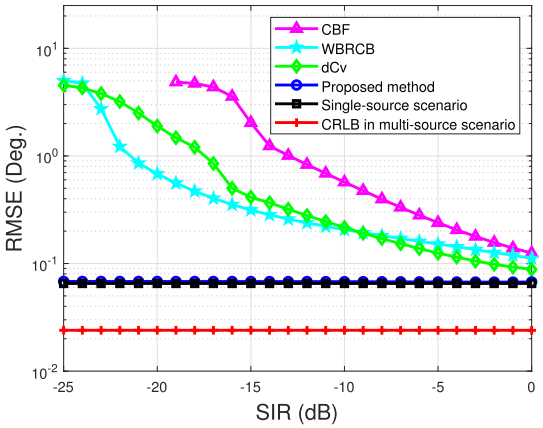

FIGURE 7. RMSE of DOA estimation versus SIR.

[−20, 15] dB. Fig. 6 presents the RMSEs of time-delay estimation versus SNR for different methods. It is evident that the RMSEs of the GCC based method, Algorithm 1, and MF based method are all decrease as the SNR increases, when the SNR surpasses the threshold SNR. However, the RMSE of the nominal based ML approach is almost independent of SNR and fixed at a constant. This is because the incorrect assumption of hydrophone coordinates is the main reason for time-delay estimation errors in this case. It is also seen that the performance of Algorithm 1 outperforms the GCC based algorithm and comparable to the MF based algorithm when the SNR surpasses −13 dB. Furthermore, the threshold SNR of Algorithm 1 is the same as that of the MF based approach and 7 dB lower than that of the GCC based approach. Note also that the RMSE of Algorithm 1 is smaller than that of the MF based method when the SNR is less than −14 dB. This is because the estimated received signal waveform contains the noises correlated with element-space data at each hydrophone, which dominated the estimated received signal waveform in this case.

Based on the above simulation analysis, we can conclude that the proposed iterative algorithm can rapidly converge to the accurate estimates of the ISF parameters. Meanwhile, it is robust to array shape distortion and array amplitude response inconsistency.

B. PERFORMANCE EVALUATION OF DOA ESTIMATION

In the following simulations, we will analyze the impact of SIR, bearing separation, and SNR on the DOA estimation performance of the proposed method in terms of RMSE. The RMSE of DOA estimation is defined as

$$RMSE_{DOA} = \sqrt{\frac{1}{N_t}\sum_{i=1}^{N_t}\left(\hat{\theta}_i - \theta\right)^2}, \tag{44}$$

where $\hat{\theta}_i$ represents the estimate of DOA at the ith trial, θ denotes the real DOA of the target signal, N_t is the number of Monte Carlo trials and is set to be 500 in the remaining simulations. The proposed method is compared with the CBF-based, WBRCB-based [28], and dCv-based [7] methods. In addition, RMSE of the estimates obtained by the beam power maximization method in the single-source scenario is also presented for comparison. For the first three cases, CRLB in the multi-source scenario is also provided as a reference.

The impact of SIR on the performance of the proposed method is investigated in the first simulation of this subsection. The target and interference signals are assumed to be incident on the array from directions of $\vartheta_1 = 40°$ and $\vartheta_2 = 20°$, respectively. The input SNR of the target signal is fixed at 0 dB and the SIR varies from 0 dB to −25 dB with a step size of −1 dB. Fig. 7 shows the RMSEs of $\hat{\vartheta}_1$ versus SIR for different methods. It is evident that the RMSEs of the CBF, WBRCB, and dCv methods increase as the SIR decreases. However, the RMSE of the proposed method is almost independent of SIR and fixed at a constant. Furthermore, the RMSE of the proposed method is smaller than those of its counterparts and close to that of the single-source scenario throughout the SIR interval. It is also worth noting that the DOA estimation accuracy of both the WBRCB and dCv methods decreases significantly when the SIR is less than −20 dB. However, the proposed method can still obtain excellent DOA estimation performance close to that of the single-source scenario, even if the SIR is as low as −25 dB. This is to be expected since when the SNR keeps unchanged, the lower is the SIR, the higher the interference-to-noise ratio (INR), and thus the higher the estimation accuracy of the element-space waveform of the interference signal.

The impact of bearing separation on the performance of the proposed method is investigated in the second simulation. The target signal arrives at the array with a DOA of $\vartheta_1 = 60°$. The interference signal is located at $\vartheta_2 = \vartheta_1 - \Delta\vartheta$, where $\Delta\vartheta$ represents the bearing separation and varies from 3° to 40° with a step size of 1°. The input SNR of the target signal is set to be 0 dB and the SIR is fixed at −15 dB. Fig. 8 illustrates the RMSEs of $\hat{\vartheta}_1$ versus bearing separation for different methods. It is observed that the proposed method outperforms comparable algorithms over the whole range of $\Delta\vartheta$. Moreover, the result of the proposed method agrees well with that of the single-source scenario when $\Delta\vartheta$ surpasses 5°.

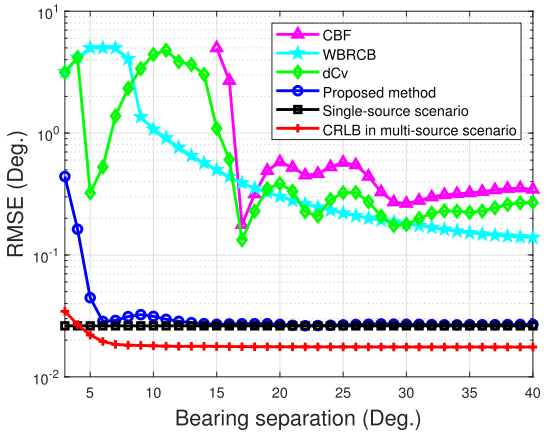

FIGURE 8. RMSE of DOA estimation versus bearing separation.

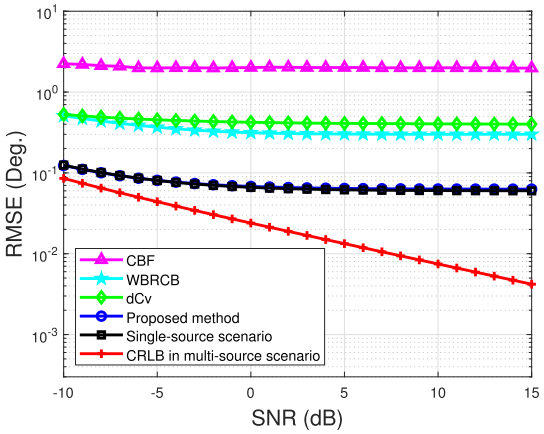

FIGURE 9. RMSE of DOA estimation versus SNR.

It is also worth noting that the RMSEs of both the CBF and dCv methods do not change monotonically with the increase of $\Delta\vartheta$. Instead, they exhibit significant fluctuations. This is due to the fact that the energy leaking from the interference beam to the target beam is not a monotonic function of $\Delta\vartheta$, as shown in (16).

The impact of SNR on the performance of the proposed method is investigated in the third simulation. The input SNR of the target signal varies over the interval $[-10, 15]$ dB. The SIR is fixed at -15 dB and the other parameters are the same as those in Fig. 7. The RMSEs of $\hat{\vartheta}_1$ versus SNR for different methods are shown in Fig. 9. It is evident that the RMSE of the proposed method is much smaller than those of its counterparts and close to that of the single-source scenario throughout the SNR range. This is because, for the CBF, WBRCB, and dCv methods, energy leakage is the main reason resulting in DOA estimation error in this scenario. It is also worth noting that the RMSEs of both the proposed method and the single-source scenario go into saturation when SNR exceeds 8 dB. The reason is that, in this case, the DOA estimation errors are mainly caused by array shape distortion.

For the fourth simulation, we consider the scenario of one target signal and three interference signals. The target signal arrives at the array with a DOA of $\vartheta_1 = 40°$. The interference signals are located at $\vartheta_2 = 20°$, $\vartheta_3 = 30°$, and $\vartheta_4 = 46°$, respectively. The input SNR of the target signal varies over the interval $[-10, 15]$ dB. The strengths of the first two interference signals are respectively 10 dB and 7 dB larger than that of the target signal, while the strength of the third interference signal is 3 dB smaller than that of the target signal. Fig. 10 shows the RMSEs of $\hat{\vartheta}_1$ versus SNR for different methods. The RMSEs of both the method in [35] (marked with Nominal based CLEAN-ISF) and its modified version (marked with Algorithm 1 based CLEAN-ISF) are also presented for comparison. For the modified version, Algorithm 1, rather than the method based on the nominal array configuration, is used to estimate the ISF parameters. It is evident that the performance of the Algorithm 1 based CLEAN-ISF method is superior to that of the Nominal based CLEAN-ISF method. This is to be expected since Algorithm 1 is robust to array shape distortion and array amplitude response inconsistency in terms of ISF parameter estimation, as discussed in Section IV-A. Note also that the proposed method outperforms the Algorithm 1 based CLEAN-ISF method in terms of DOA estimation accuracy. This is because the CLEAN-ISF method is achieved by sequentially removing the interference signals from the received hydrophone data in order of descending strength, one at a time. The signal removal is ended once the target signal is detected from the updated element-space data. Thus, the interference signals weaker than the target signal are not removed and still remain in the element-space data. However, the DOA estimation accuracy of the target signal is also, to some extent, affected by the interference signals weaker than itself, particularly when their strengths are comparable or the bearing separation is small. On the other hand, during the sequential signal removal, the estimation accuracy of ISF parameters of the previously detected interference signals are also affected by the signals that have not yet been detected. Thus, the element-space waveforms of interference signals are not properly removed, which can degrade the DOA estimation accuracy of the target signal to some extent. Both of the influences mentioned above are significantly mitigated by the proposed method, which follows a coarse-to-fine procedure for DOA estimation.

Simulation results presented above show that, in the presence of multiple sources and array shape distortion, the proposed method outperforms its counterparts in terms of estimation accuracy. Meanwhile, the DOA estimation performance of the proposed method is close to that obtained in the single-source scenario, even if the SIR is as low as -25 dB.

V. EXPERIMENT OF SEA TRIAL DATA

In this section, the performance of the proposed method is evaluated with real data collected at sea. Fig. 11 demonstrates the schematic diagram of the sea trial, conducted in the South China Sea. As shown in Fig. 11, the depths of the sea, the acoustic source and the receiving array are 105 m, 20 m

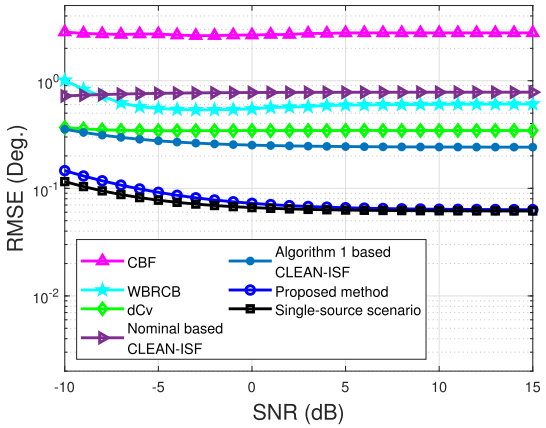

FIGURE 10. RMSE of DOA estimation versus SNR in the presence of one target signal and three interference signals.

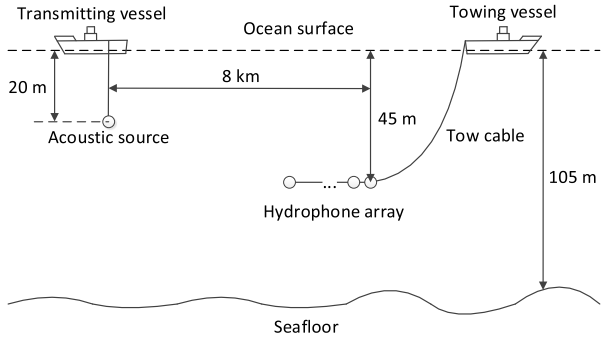

FIGURE 11. Schematic diagram of the sea trial.

and 45 m, respectively. The transmitting vessel is anchored, and a wideband signal is transmitted from the acoustic source with a spectrum level of 130 dB at 1 kHz. The sound speed profile (SSP) obtained in the sea trial area shows a weak negative gradient. The towing vessel runs according to the predesigned route with a speed of 6 knots. The distance between the acoustic source and the receiving array is about 8 km. The length of the tow cable is 700 m and the data is collected from a towed array comprising of 100 elements with inter-element spacing 0.8 m. The sampling frequency f_s, time analysis window length T, and lower and upper bounds of the analysis frequency band are the same as those in the simulations.

The bearing time record (BTR) calculated using 32 hydrophones based on the CBF, WBRCB, dCv, and the proposed method are shown in Fig. 12(a), 12(b), 12(c), and 12(d), respectively. For reference, the BTR calculated utilizing 100 hydrophones based on the dCv is shown in Fig. 12(e). As seen from Fig. 12(e), the number of sources is seven. The target signal impinges on the array from direction around 37° and the towing vessel interference is located at around 17°. These are consistent with the results calculated using the Global-Position-System (GPS) coordinates of the transmitting and towing vessels and the orientation of the hydrophone array. However, for Fig. 12(a), it is difficult to identify the trajectory of the target signal from the surrounding interference sources, since the beam power

TABLE 2. RMSE of DOA estimation results of sea trial data.

	WBRCB	dCv	Proposed method
RMSE (Deg.)	0.891	0.496	0.221

peak of the target signal is masked by the high sidelobes of the towing vessel interference. As for Fig. 12(b) and 12(c), although the energy leakages are reduced to some extent, the beam power peaks of the target signal are still severely damaged. It is worth noting that the only trajectory visible in Fig. 12(d) belongs to the target signal. This is expected since the proposed method reconstructs the element-space data to approach the received hydrophone data of a single-source scenario, containing only the target signal component. The profiles of the results at $t = 100$ s are presented in Fig. 12(f). It is evident that the maximum peak of the beam power sample sequence, calculated exploiting reconstructed element-space data, is associated with the target signal. Its abscissa agrees well with the target DOA obtained from Fig. 12(e).

The DOA estimation results obtained from Fig. 12(b), 12(c), 12(d), and 12(e) are presented in Fig. 13. Note that limited orientation accuracy of the towed array, provided by the attitude sensor, makes it difficult to obtain the high-accuracy target DOA exploiting the GPS coordinates and array orientation in the sea trial environment. Comparing Fig. 12(e) with Fig. 12(a), 12(b), and 12(c) suggests that the dCv beam power, calculated utilizing 100 hydrophones, exhibits significantly lower sidelobes and narrower beamwidths. As a result, the target trajectory is clear throughout the time frame and the obtained estimates of DOA exhibit higher estimation accuracy. As such, the estimates of DOA obtained from Fig. 12(e) can be used as the references to evaluate the performance of the proposed method. From Fig. 13, it is evident that the estimates of DOA obtained by the proposed method agree well with the references throughout the time frame. In contrast, the estimates produced by both WBRCB and dCv methods exhibit significant deviations from the reference in some time frames. The DOA estimation accuracy is measured through RMSE and the obtained results are listed in Table 2. It can be seen that the proposed method outperforms the WBRCB and dCv methods, which is consistent with the BTR presented in Fig. 12.

These results suggest that the proposed method still maintains better effectiveness and higher robustness compared to its counterparts, even though the number of sources is as many as seven and the target signal is contaminated by real ocean ambient noise. It is worth noting that the signals from different sources are not totally uncorrelated with each other, especially for those encountered in a towed array sonar system [47]–[49]. The magnitudes of correlation are related to the type and working conditions of sources, the frequency and bandwidth of signals, and the underwater environment [50]–[52]. For the proposed ESDR-based wideband DOA estimation algorithm, the influence of correlation among the signals mainly lies in the time-delay estimation based on cross-correlations between the estimated received signal

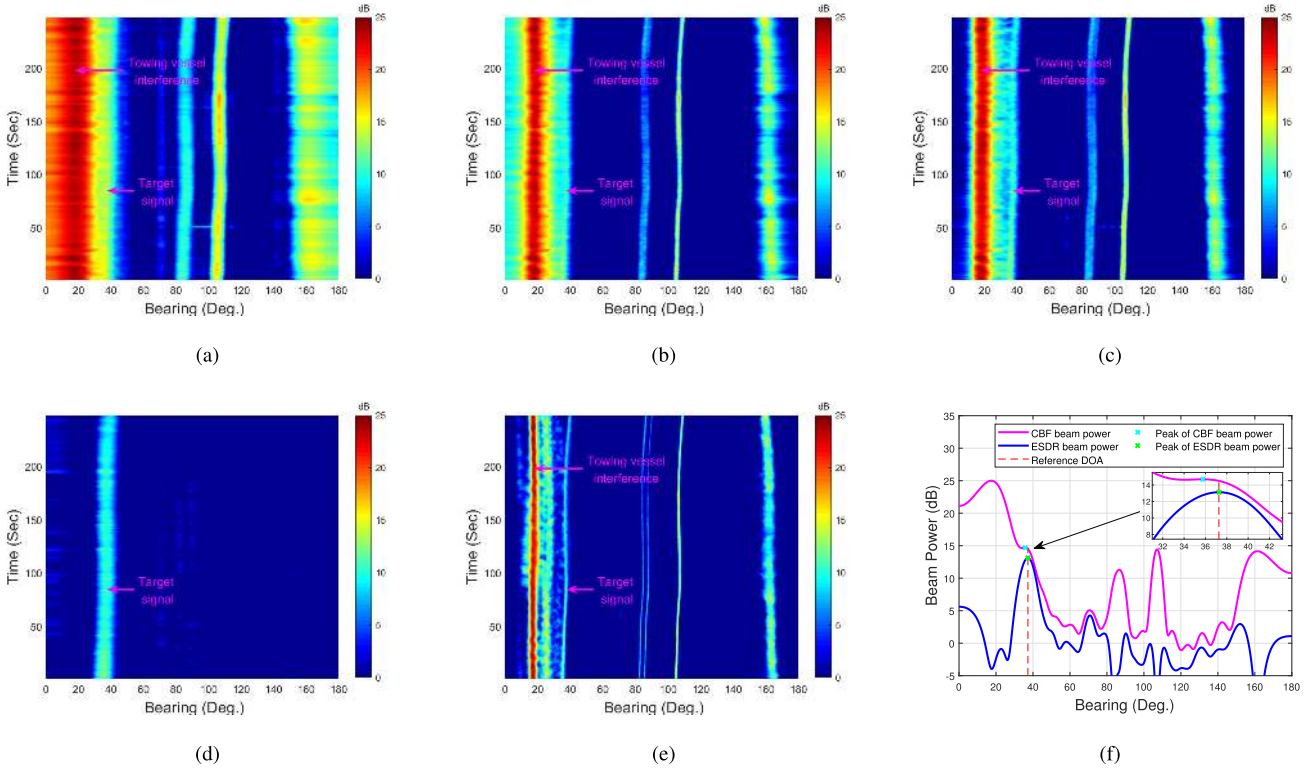

FIGURE 12. BTR calculated using 32 hydrophones based on (a) CBF, (b) WBRCB, (c) dCv, (d) the proposed method. (e) BTR calculated utilizing 100 hydrophones based on dCv. (f) Profile of the results at $t = 100$ s.

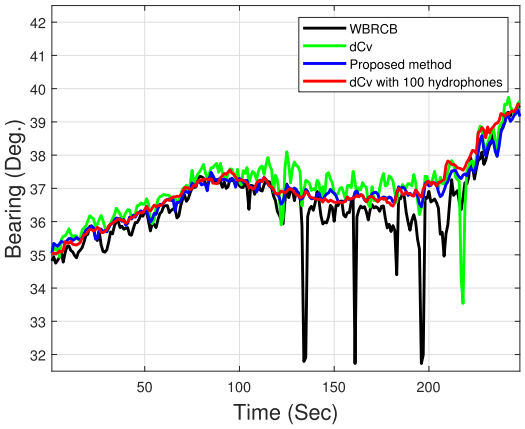

FIGURE 13. DOA estimation results of sea trial data.

waveform and the element-space data of every hydrophone. This influence is mitigated significantly in the proposed method due to the magnitudes of all the signals, except the one currently considered, are much decreased by the signal removal and beamforming.

VI. CONCLUSION

In this paper, a robust ESDR-based wideband DOA estimation method is proposed to acquire the accurate bearings of the weak signals in a multi-source environment. The proposed method first directly reconstructs the element-space data to approach the received hydrophone data in a single-source scenario, containing only the SOI. Thus, it can completely eliminate or significantly reduce the unacceptable energy leaking from the interference beams to the target beam. A refined estimate of DOA is then obtained based on the reconstructed element-space data. Both simulation and at-sea experimental results verify the advantages of the proposed method over the WBRCB based and dCv based DOA estimation methods. In addition, the proposed method is particularly suitable for the scenario of DOA estimation with a towed array, where strong interference sources and array shape distortion coexist. The future work will consider the analytical derivation for the DOA estimation accuracy of the proposed method and extend this method to the scenarios with lower SNR.

ACKNOWLEDGMENT

The authors would like to thank the anonymous reviewers and the editor Dr. Jiajia Jiang for their careful reading and valuable comments.

REFERENCES

[1] H. L. Van Trees, *Optimum Array Processing: Part IV of Detection, Estimation, and Modulation Theory*. Hoboken, NJ, USA: Wiley, 2004.
[2] W. Liu and S. Weiss, *Wideband Beamforming: Concepts and Techniques*. Hoboken, NJ, USA: Wiley, 2010.
[3] F. Wen, Z. Zhang, K. Wang, G. Sheng, and G. Zhang, "Angle estimation and mutual coupling self-calibration for ULA-based bistatic MIMO radar," *Signal Process.*, vol. 144, pp. 61–67, Mar. 2018.
[4] L. C. Godara, "Application of antenna arrays to mobile communications. II. Beam-forming and direction-of-arrival considerations," *Proc. IEEE*, vol. 85, no. 8, pp. 1195–1245, Aug. 1997.
[5] X. Wang, L. Wang, X. Li, and G. Bi, "Nuclear norm minimization framework for DOA estimation in MIMO radar," *Signal Process.*, vol. 135, pp. 147–152, Jun. 2017.

[6] L. Wan, G. Han, J. Jiang, J. J. P. C. Rodrigues, N. Feng, and T. Zhu, "DOA estimation for coherently distributed sources considering circular and noncircular signals in massive MIMO systems," *IEEE Syst. J.*, vol. 11, no. 1, pp. 41–49, Mar. 2017.
[7] T. C. Yang, "Deconvolved conventional beamforming for a horizontal line array," *IEEE J. Ocean. Eng.*, vol. 43, no. 1, pp. 160–172, Jan. 2018.
[8] J. Capon, "High-resolution frequency-wavenumber spectrum analysis," *Proc. IEEE*, vol. 57, no. 8, pp. 1408–1418, Aug. 1969.
[9] R. Schmidt, "Multiple emitter location and signal parameter estimation," *IEEE Trans. Antennas Propag.*, vol. AP-34, no. 3, pp. 276–280, Mar. 1986.
[10] L. Wan, Y. Sun, L. Sun, Z. Ning, and J. J. P. C. Rodrigues, "Deep learning based autonomous vehicle super resolution DOA estimation for safety driving," *IEEE Trans. Intell. Transp. Syst.*, early access, Aug. 21, 2020, doi: 10.1109/TITS.2020.3009223.
[11] D. P. Wipf and B. D. Rao, "An empirical Bayesian strategy for solving the simultaneous sparse approximation problem," *IEEE Trans. Signal Process.*, vol. 55, no. 7, pp. 3704–3716, Jul. 2007.
[12] S. F. Cotter, B. D. Rao, K. Engan, and K. Kreutz-Delgado, "Sparse solutions to linear inverse problems with multiple measurement vectors," *IEEE Trans. Signal Process.*, vol. 53, no. 7, pp. 2477–2488, Jul. 2005.
[13] D. Malioutov, M. Cetin, and A. S. Willsky, "A sparse signal reconstruction perspective for source localization with sensor arrays," *IEEE Trans. Signal Process.*, vol. 53, no. 8, pp. 3010–3022, Aug. 2005.
[14] C. Liu, Y. V. Zakharov, and T. Chen, "Broadband underwater localization of multiple sources using basis pursuit de-noising," *IEEE Trans. Signal Process.*, vol. 60, no. 4, pp. 1708–1717, Apr. 2012.
[15] Q. Wu and S. Fang, "High-resolution DOA estimation in the underwater radiated noise based on sparse Bayesian learning," in *Proc. INTER-NOISE NOISE-CON Congr. Conf.*, 2016, pp. 2862–3857.
[16] D. Meng, X. Wang, M. Huang, L. Wan, and B. Zhang, "Robust weighted subspace fitting for DOA estimation via block sparse recovery," *IEEE Commun. Lett.*, vol. 24, no. 3, pp. 563–567, Mar. 2020.
[17] A. Das and T. J. Sejnowski, "Narrowband and wideband off-grid direction-of-arrival estimation via sparse Bayesian learning," *IEEE J. Ocean. Eng.*, vol. 43, no. 1, pp. 108–118, Jan. 2018.
[18] A. Das, "Theoretical and experimental comparison of off-grid sparse Bayesian direction-of-arrival estimation algorithms," *IEEE Access*, vol. 5, pp. 18075–18087, 2017.
[19] A. Das, "A Bayesian sparse-plus-low-rank matrix decomposition method for direction-of-arrival tracking," *IEEE Sensors J.*, vol. 17, no. 15, pp. 4894–4902, Aug. 2017.
[20] M.-H. Wei, W. R. Scott, and J. H. McClellan, "Jointly sparse vector recovery via reweighted l_1 minimization," in *Proc. IEEE Int. Conf. Acoust., Speech Signal Process. (ICASSP)*, Mar. 2012, pp. 3929–3932.
[21] Z.-M. Liu, Z.-T. Huang, and Y.-Y. Zhou, "Direction-of-arrival estimation of wideband signals via covariance matrix sparse representation," *IEEE Trans. Signal Process.*, vol. 59, no. 9, pp. 4256–4270, Sep. 2011.
[22] Z.-M. Liu, Z.-T. Huang, and Y.-Y. Zhou, "Sparsity-inducing direction finding for narrowband and wideband signals based on array covariance vectors," *IEEE Trans. Wireless Commun.*, vol. 12, no. 8, pp. 1–12, Aug. 2013.
[23] Q. Wu, P. Xu, T. Li, and S. Fang, "Feature enhancement technique with distorted towed array in the underwater radiated noise," in *Proc. INTER-NOISE NOISE-CON Congr. Conf.*, 2017, pp. 2999–3996.
[24] J. L. Odom and J. L. Krolik, "Passive towed array shape estimation using heading and acoustic data," *IEEE J. Ocean. Eng.*, vol. 40, no. 2, pp. 465–474, Apr. 2015.
[25] I. W. Schurman, "Reverberation rejection with a dual-line towed array," *IEEE J. Ocean. Eng.*, vol. 21, no. 2, pp. 193–204, Apr. 1996.
[26] S. G. Lemon, "Towed-array history, 1917–2003," *IEEE J. Ocean. Eng.*, vol. 29, no. 2, pp. 365–373, Apr. 2004.
[27] J. Li, P. Stoica, and Z. Wang, "On robust capon beamforming and diagonal loading," *IEEE Trans. Signal Process.*, vol. 51, no. 7, pp. 1702–1715, Jul. 2003.
[28] S. D. Somasundaram, "Wideband robust capon beamforming for passive sonar," *IEEE J. Ocean. Eng.*, vol. 38, no. 2, pp. 308–322, Apr. 2013.
[29] Y. Yang, Y. Zhang, and L. Yang, "Wideband sparse spatial spectrum estimation using matrix filter with nulling in a strong interference environment," *J. Acoust. Soc. Amer.*, vol. 143, no. 6, pp. 3891–3898, Jun. 2018.
[30] L. Wan, X. Kong, and F. Xia, "Joint range-Doppler-angle estimation for intelligent tracking of moving aerial targets," *IEEE Internet Things J.*, vol. 5, no. 3, pp. 1625–1636, Jun. 2018.
[31] J. A. Högbom, "Aperture synthesis with a non-regular distribution of interferometer baselines," *Astron. Astrophys. Suppl.*, vol. 15, pp. 417–426, Jun. 1974.
[32] H. Deng, "Effective CLEAN algorithms for performance-enhanced detection of binary coding radar signals," *IEEE Trans. Signal Process.*, vol. 52, no. 1, pp. 72–78, Jan. 2004.
[33] O. Akhdar, M. Mouhamadou, D. Carsenat, C. Decroze, and T. Monediere, "A new CLEAN algorithm for angle of arrival denoising," *IEEE Antennas Wireless Propag. Lett.*, vol. 8, pp. 478–481, 2009.
[34] M. K. Robert and S. P. Beerens, "Adaptive beamforming algorithms for tow ship noise canceling," in *Proc. UDT*, 2002, pp. 1–11.
[35] Q. Li, C. Wei, and S. Xue, "Iterative inverse beamforming algorithm and its application in multiple targets detection of passive sonar," *Chin. J. Acoust.*, vol. 36, no. 2, pp. 208–216, 2017.
[36] Q. Li, *Digital Sonar Design in Underwater Acoustics: Principles and Applications*. New York, NY, USA: Springer-Verlag, 2012.
[37] Z.-M. Liu and Y.-Y. Zhou, "A unified framework and sparse Bayesian perspective for direction-of-arrival estimation in the presence of array imperfections," *IEEE Trans. Signal Process.*, vol. 61, no. 15, pp. 3786–3798, Aug. 2013.
[38] J. Jiang, F. Duan, J. Chen, Z. Chao, Z. Chang, and X. Hua, "Two new estimation algorithms for sensor gain and phase errors based on different data models," *IEEE Sensors J.*, vol. 13, no. 5, pp. 1921–1930, May 2013.
[39] V. H. MacDonald and P. M. Schultheiss, "Optimum passive bearing estimation in a spatially incoherent noise environment," *J. Acoust. Soc. Amer.*, vol. 46, no. 1A, pp. 37–43, Jul. 1969.
[40] S. M. Kay, *Fundamentals of Statistical Signal Processing: Estimation Theory*, vol. I. Upper Saddle River, NJ, USA: Prentice-Hall, 1993.
[41] S. Djukanović, T. Popović, and A. Mitrović, "Precise sinusoid frequency estimation based on parabolic interpolation," in *Proc. 24th Telecommun. Forum (TELFOR)*, Nov. 2016, pp. 1–4.
[42] S. Djukanović and V. Popović-Bugarin, "Efficient and accurate detection and frequency estimation of multiple sinusoids," *IEEE Access*, vol. 7, pp. 1118–1125, 2019.
[43] H. Messer, "The potential performance gain in using spectral information in passive detection/localization of wideband sources," *IEEE Trans. Signal Process.*, vol. 43, no. 12, pp. 2964–2974, Dec. 1995.
[44] D. A. Abraham, *Underwater Acoustic Signal Processing: Modeling, Detection, and Estimation*. New York, NY, USA: Springer-Verlag, 2019.
[45] E. Weinstein and A. Weiss, "Fundamental limitations in passive time-delay estimation—Part II: Wide-band systems," *IEEE Trans. Acoust., Speech, Signal Process.*, vol. ASSP-32, no. 5, pp. 1064–1078, Oct. 1984.
[46] C. Knapp and G. Carter, "The generalized correlation method for estimation of time delay," *IEEE Trans. Acoust., Speech, Signal Process.*, vol. ASSP-24, no. 4, pp. 320–327, Aug. 1976.
[47] A. Das, "Deterministic and Bayesian sparse signal processing algorithms for coherent multipath directions-of-arrival (DOAs) estimation," *IEEE J. Ocean. Eng.*, vol. 44, no. 4, pp. 1150–1164, Oct. 2019.
[48] A. Das, W. S. Hodgkiss, and P. Gerstoft, "Coherent multipath direction-of-arrival resolution using compressed sensing," *IEEE J. Ocean. Eng.*, vol. 42, no. 2, pp. 494–505, Apr. 2017.
[49] P. Gerstoft, W. S. Hodgkiss, W. A. Kuperman, H. Song, M. Siderius, and P. L. Nielsen, "Adaptive beamforming of a towed array during a turn," *IEEE J. Ocean. Eng.*, vol. 28, no. 1, pp. 44–54, Jan. 2003.
[50] R. J. Urick, *Principles of Underwater Sound*, 3rd ed. New York, NY, USA: McGraw-Hill, 1983.
[51] N. M. Carbone and W. S. Hodgkiss, "Effects of tidally driven temperature fluctuations on shallow-water acoustic communications at 18 kHz," *IEEE J. Ocean. Eng.*, vol. 25, no. 1, pp. 84–94, Jan. 2000.
[52] W. S. Hodgkiss, W. A. Kuperman, and D. E. Ensberg, "Channel impulse response fluctuations at 6 kHz in shallow water," in *Impact of Littoral Environmental Variability of Acoustic Predictions and Sonar Performance*. New York, NY, USA: Springer-Verlag, 2002, pp. 295–302.

CHUANQI ZHU (Student Member, IEEE) received the B.S. degree in communication engineering from Northeast Forestry University, Harbin, China, in 2012, and the M.S. degree in signal and information processing from Southeast University, Nanjing, China, in 2016, where he is currently pursuing the Ph.D. degree with the Key Laboratory of Underwater Acoustic Signal Processing, Ministry of Education. His research interests include target detection and parameter estimation, high-fidelity target signal reconstruction, and feature extraction.

SHILIANG FANG received the M.S. and Ph.D. degrees from Southeast University, Nanjing, China, in 1986 and 2009, respectively. He is currently a Professor with the Key Laboratory of Underwater Acoustic Signal Processing, Ministry of Education, Southeast University. As the Committee Member of underwater acoustic branch of Acoustical Society of China, his research interests include signal processing, target detection and parameter estimation, and underwater target classification.

QISONG WU received the B.S. and Ph.D. degrees from Xidian University, Xi'an, China, in 2005 and 2010, respectively. He was a Postdoctoral Associate with Duke University, Durham, NC, USA, from 2010 to 2013, and Villanova University, Villanova, PA, USA, from 2013 to 2015. He is currently an Associate Professor with the Key Laboratory of Underwater Acoustic Signal Processing of Ministry of Education, Southeast University. His research interests include sonar signal processing, radar signal processing, and the sparse Bayesian learning.

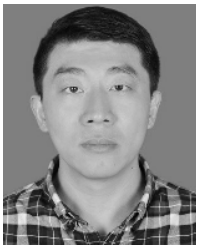

LIANG AN received the B.S. degree in information engineering and the M.S. and Ph.D. degrees in signal and information processing from Southeast University, Nanjing, China, in 2001, 2006, and 2009, respectively. He is currently a Professor with the School of Information Science and Engineering, Southeast University. As the Committee Member of underwater acoustic branch of Acoustical Society of China, his research interests include underwater acoustic localization and target classification.

XINWEI LUO received the B.S., M.S., and Ph.D. degrees from Southeast University, Nanjing, China, in 2001, 2006, and 2013, respectively. He is currently an Associate Professor with the Key Laboratory of Underwater Acoustic Signal Processing, Ministry of Education, Southeast University. His research interests include acoustic signal processing, target detection, parameter estimation, and underwater target classification.